5-2015

Uplift rate of marine terraces and anticlinal growth along the North Canterbury fold and thrust belt, New Zealand

Mary Kate Stewart
Trinity University, mstewar1@trinity.edu

Uplift rate of marine terraces and anticlinal growth along the North Canterbury fold and thrust belt, New Zealand

Mary Kate Stewart

A DEPARTMENT HONORS THESIS SUBMITTED TO THE
DEPARTMENT OF GEOSCIENCES AT TRINITY UNIVERSITY
IN PARTIAL FULFILLMENT OF THE REQUIREMENTS FOR GRADUATION WITH DEPARTMENTAL HONORS

May 2016

_____
Thomas Gardner, Thesis Advisor

_____
Diane Smith, Department Chair

_____
Sheryl Tynes, AVPAA

Student Agreement

I grant Trinity University (“Institution”), my academic department (“Department”), and the Texas Digital Library ("TDL") the non-exclusive rights to copy, display, perform, distribute and publish the content I submit to this repository (hereafter called "Work") and to make the Work available in any format in perpetuity as part of a TDL, Institution or Department repository communication or distribution effort.

I understand that once the Work is submitted, a bibliographic citation to the Work can remain visible in perpetuity, even if the Work is updated or removed.

I understand that the Work's copyright owner(s) will continue to own copyright outside these non-exclusive granted rights.

I warrant that:

1) I am the copyright owner of the Work, or
2) I am one of the copyright owners and have permission from the other owners to submit the Work, or
3) My Institution or Department is the copyright owner and I have permission to submit the Work, or
4) Another party is the copyright owner and I have permission to submit the Work.

Based on this, I further warrant to my knowledge:

1) The Work does not infringe any copyright, patent, or trade secrets of any third party,
2) The Work does not contain any libelous matter, nor invade the privacy of any person or third party, and
3) That no right in the Work has been sold, mortgaged, or otherwise disposed of, and is free from all claims.

I agree to hold TDL, Institution, Department, and their agents harmless for any liability arising from any breach of the above warranties or any claim of intellectual property infringement arising from the exercise of these non-exclusive granted rights.”

I choose the following option for sharing my thesis (required):

[X] Open Access (full-text discoverable via search engines)
[ ] Restricted to campus viewing only (allow access only on the Trinity University campus via digitalcommons.trinity.edu)

Acknowledgements

Let's have a round of applause for all the people involved in the thesis process: Tom Gardner, my thesis advisor and mentor, the professor who helped foster a passion for geoscience, the professor who has developed the uncanny ability to distinguish between "smart mouth" Mary Kate and "good idea" Mary Kate, and the professor who allowed me to travel with him to New Zealand; David Oakley, a Ph. D student at Penn State for trusting my ability as a scientist to contribute a small part to his dissertation; Mr. MacIntosh, Mr. Heard and Mr. Moyer, the landowners who graciously let us wander around their property; the entire Trinity University geoscience faculty and staff for providing encouragement throughout my four years as a student; my family, Randall, Jeannine, and Carmen Stewart, and Sage Cunningham for listening to exasperated phone-calls; and Kirk Gulliver for providing me with apple juice when I was temporarily living in the geo lab.

Abstract

This study measures the uplift rates of a flight of marine terraces along the Glenafric coastal region of the South Island of New Zealand, which will provide a context for how local fold growth in the North Canterbury fold and thrust belt (NCFTB) contributes to local uplift rates. Several methods were used to measure uplift rate of the marine terraces: 1) collecting shell samples for AAR dating in order to refine terrace ages; 2) use of DGPS surveys to collect the elevations of marine terrace inner edges and possible marine terrace erosional surfaces; 3) creating several cross-sections based on the DGPS surveys to refine terrace boundaries; and 4) calculating the uplift rate of all marine terraces along the North Canterbury fold and thrust belt to determine possible structural influence on local uplift.

Amino acid rasterization (AAR) and optically stimulated luminescence (OSL) dating techniques were used to date the youngest terrace, Qt_3, at ~100 ka, placing Qt_3 at marine isotope stage (MIS) 5c. Correlations to sea level highstands from inner edge elevation projections from the cross-sections were used to date Qt_2 at ~120 ka and Qt_1 at ~210 ka. Correlations of inner edge elevations to the Cass and Montserrat anticlines show that inner edges closest to the anticlinal axis were generally higher in elevation than points farther from the anticlinal axis. However, this was not the case for all GPS survey points as GPS surveys in the southern region of the field exhibit low elevations and are in close proximity to the anticlinal crest. Therefore another mechanism must contribute to marine terrace uplift as well.

Topographic profiles created from LIDAR and calculated uplift rates provide evidence of marine terrace southwestward tilting, following the southwestward plunge of the Cass anticline and southwestward propagation of the Hamilton fault and other thrust faults in the NCFTB. The GPS points with the highest uplift rates, 1.0 -1.3 m/kyr, are closest to the structural culmination of the Cass or Montserrat anticline, or belong to the oldest terrace, Qt1 (MIS 7a), and have therefore experienced fold influence and uplift for the longest period of time. Proximity to the structural culmination of each anticline, not proximity to the anticlinal axis, is therefore the dominate control on marine terrace uplift rate.

Table of Contents

List of Figures

List of Tables

Introduction

Oblique convergence characterizes the South Island of New Zealand as the Pacific plate migrates southwest relative to the Australian plate at a rate of 41 mm/yr (Figure 1). Convergence between the Challenger Plateau on the Australian plate and the Chatham Rise and Campbell Plateau on the Pacific plate, result in compression in the upper plate and the development of the North Canterbury fold and thrust belt (NCFTB) in the northern end of the South Island (Figure 2). The patterns and rates of deformation in forearc fold and thrust belts are controlled primarily by plate kinematics and variations in thickness and density of the converging plates; therefore, this tectonic setting also controls the rates and style of deformation in the NCFTB. The goal of this study is to measure uplift rates of a flight of marine terraces and relate the measured uplift to anticlinal growth in the North Canterbury fold and thrust belt in response to plate convergence.

Assigning ages to marine terraces is critical in order to constrain the rates of deformation and timing of folding, especially since very few ages have been assigned to terraces along the Glenafric coast. This study will improve upon previously mapped terraces that have poor elevation and age control (Carr, 1970; Yousif, 1987), and will ultimately allow for better terrace correlation and a more accurate estimation of rates of uplift. The goals of this study are to:

- Determine accurate terrace elevations using differentially corrected DGPS surveys with a Trimble GPS receiver;
- Define terraces using the DGPS surveys;
- Refine age estimates of the marine terraces using amino acid rasterization (AAR) and optically stimulated luminescence (OSL) data;
- Refine descriptions of local Quaternary stratigraphy of marine terraces;
- Calculate the local uplift rate of marine terraces along the NCFTB and determine the possible structural influences on local uplift.

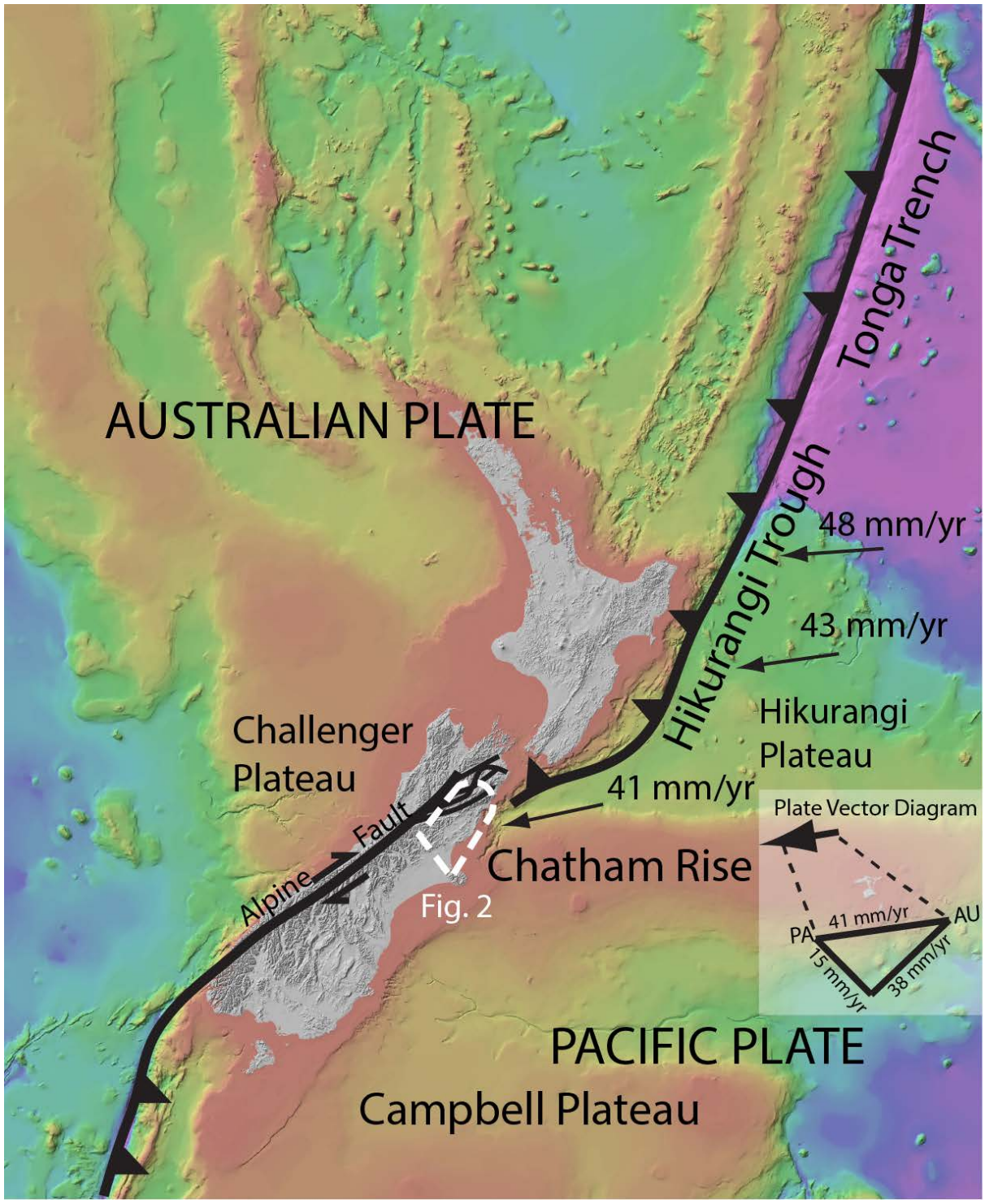

Figure 1. Tectonic setting and map of New Zealand showing the bathymetry and relative plate motions of the Australian and Pacific plate. Republished with permission of Oxford Journals from (Geologically current plate motions, Demets, Geophysical Journal International, 181).

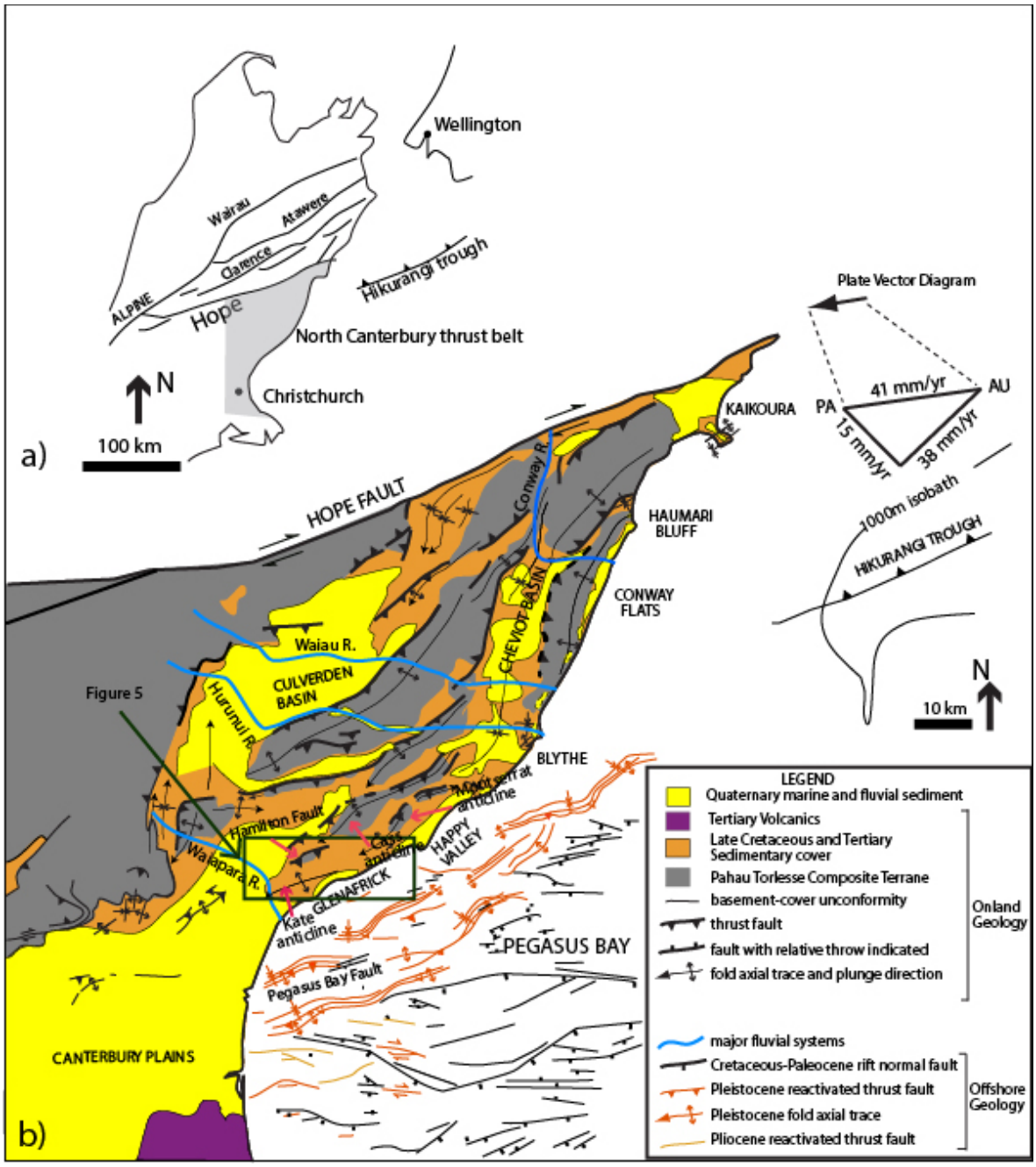

Figure 2. Geologic map of the Marlborough region of the South Island. The map includes structures associated with the North Canterbury fold and thrust belt, both onshore (modified from the Qmap of Christchurch) and offshore (modified from Barnes et al, 1996, 2011). The velocity triangle represents relative plate motion as well as the velocity components parallel and perpendicular to the plate boundary (Demets et al., 2010). The region of study for this research, Glenafric, is highlighted in the green box.

Background

Strain partitioning occurs as a result of the continental crust of the Pacific plate being unable to subduct underneath the continental crust of the Australian plate. As a result, the Pacific plate delaminates (Furlong and Kemp, 2009; Walcott, 1998; Figure 3) as the continental crust compresses against the Hope Fault (a splay of the Alpine Fault) by the plate boundary and the lower crust and upper mantle attempt to subduct beneath the Australian plate, creating a margin-orthogonal contractional component (~15 mm/yr) in the NCFTB (Walcott 1998). The NCFTB and its associated faults (Hamilton Fault) and folds (Kate and Cass Anticlines) are propagating southwestward in response to the migration of the Pacific plate. Strike-slip motion occurs along the Alpine Fault (~38 mm/yr) and the faults of the Marlborough system; however, the primary focus of this study is on the

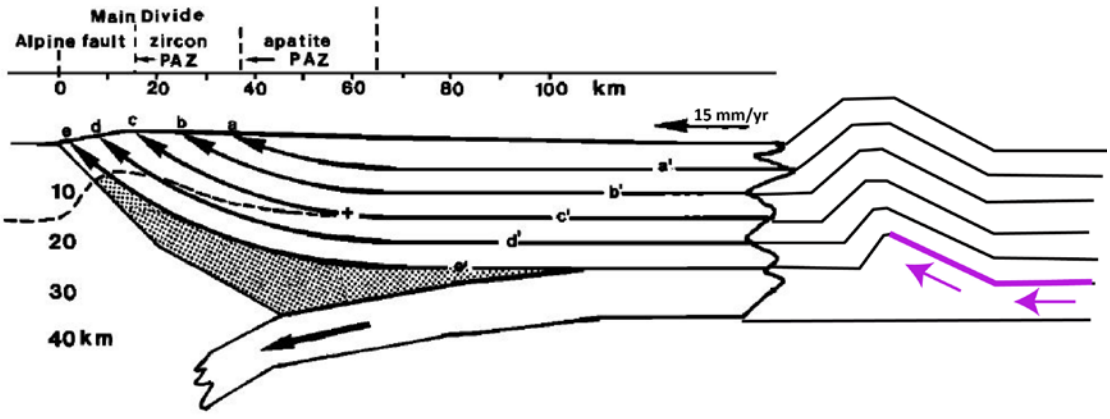

Figure 3. Deformation of the Pacific plate as a result of strain partitioning and the consequent creation of folding, specifically the North Canterbury fold and thrust belt, from thrust faulting. Republished with permission of American Geophysical Union, from (Modes of oblique compressions: late Cenozoic tectonics of the South Island of New Zealand, Walcott, 36, 1, 1998); permission conveyed through Copyright Clearance Center, Inc.

compressional component.

Northeast-southwest trending folds 20km offshore of Pegasus Bay have been inferred from seismic data to overlie a system of blind southeast dipping thrust faults that accommodate 9-11km of crustal shortening between the Hope Fault and Pacific coast. Based on the asymmetrical geometries of these folds, as well as their association with low angle blind thrust faults, these offshore folds are characterized as fault- propagation folds. The deposition, folding, and uplift of 12 offshore stratigraphic units have occurred progressively for the past 0.75 Ma. Coastal uplift rates have helped to constrain the rate of deformation and timing of folding allowing for estimation of fold amplitude growth rates and blind thrust fault slip rates. (Figure 2, Barnes, 1996, 2011).

The stratigraphy of the offshore folds is comparable to the onshore folds. Offshore fold stratigraphy is characterized by a sedimentary drift sequence that overlies the Late Jurassic- Early Cretaceous Torlesse Terrane, which composes the north Canterbury basement. This drift sequence is composed of alternating layers of clastic fluvial and marine deposits, ranging in age from Late Pliocene to present day (Figure 4). Stratigraphic units 11-9 range in thickness from 0-20 m, thinning over anticline crests, indicating active fold growth during deposition of the units (Barnes, 1995; 1996; 2011). Much like the offshore folds, the Pahau Torlesse Terrane, deposited in the Early Cretaceous, comprises the north Canterbury basement and is overlain by a drift sequence of alternating layers of clastic non-marine and shallow shelf marine sediments (Oligocene-Pliocene) for onshore folds (Figure 5). Overlying the drift sequence is a series of Quaternary alluvial and marine terrace deposits.

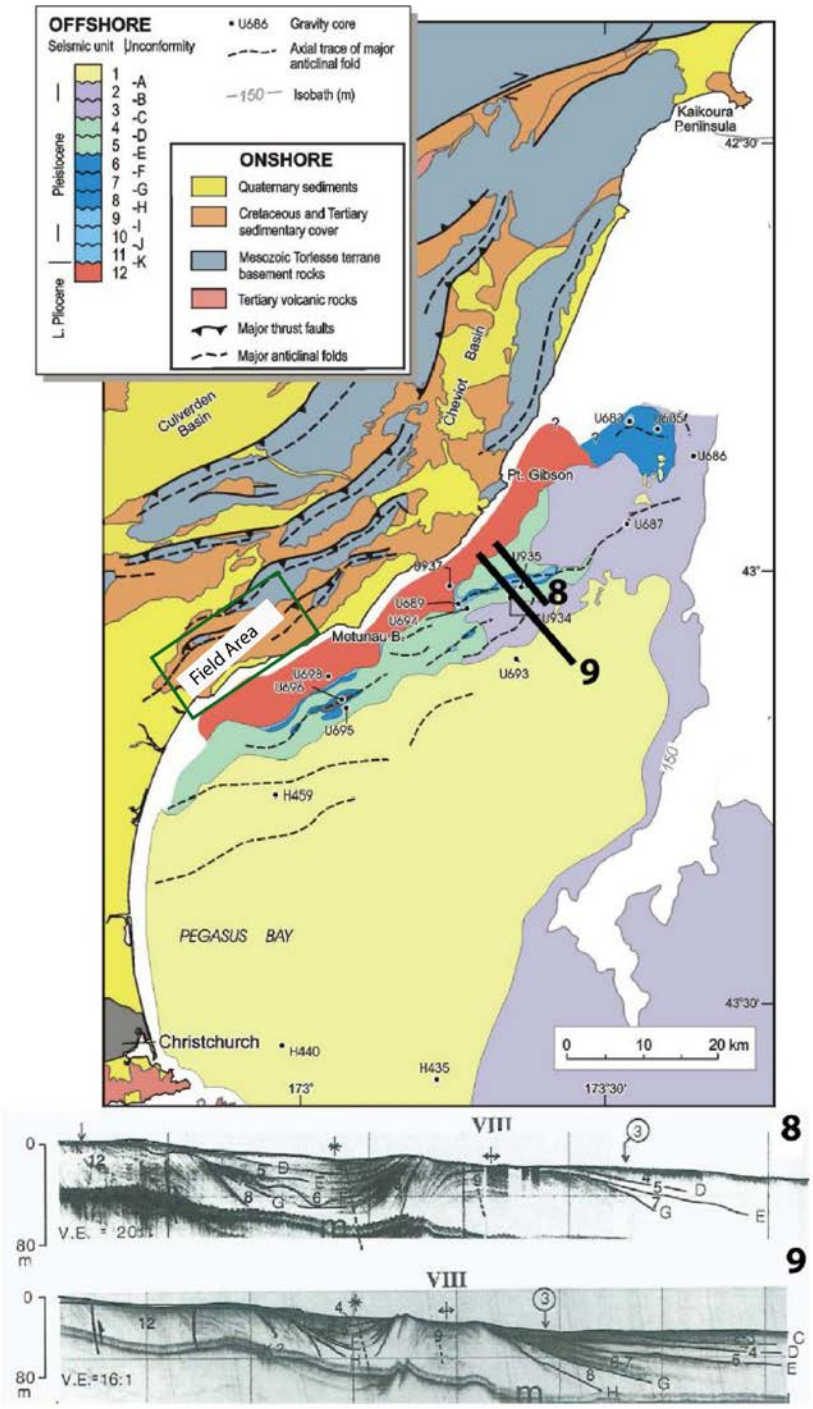

Figure 4. Offshore and onshore NCFTB geologic map of 12 stratigraphic units from the North Canterbury shelf and coastal region with 3.5 kHz profiles of active submarine folds. Reprinted from (Barnes, Submarine faulting beneath Pegasus Bay, offshore Christchurch, Tectonics, 2011).

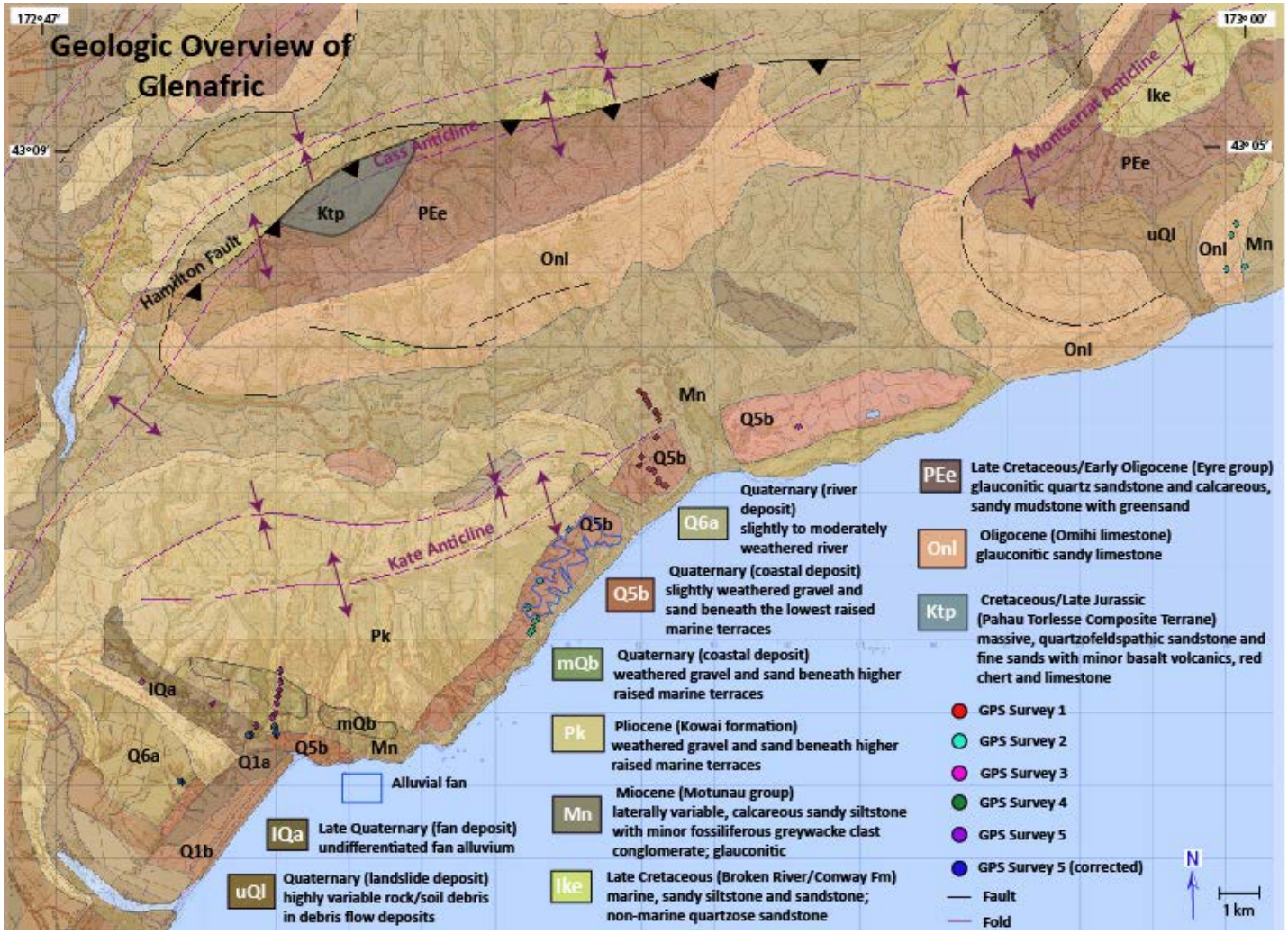

Figure 5: Geologic map of Glenafric. Faults, geologic structures, and geologic units pertinent to the study are labeled and highlighted respectively (taken from http://www.gns.cri.nz/). GPS surveys are labeled as well. See Figure 2 for location.

Field Area

The field area of this study extends south along the coast of the South Island of New Zealand from the landslide area north of Glenafric to Teviotdale. Figure 6 provides a general overview of the field area including the most extensive marine terrace and adjacent fold (the hill in the background). Figure 6a shows that both the marine terrace and fold plunge toward the southwest, an effect of greater contraction in the northeast. Figure 2 verifies this plunge as it shows that, in general, the thrust faults converge in the northeast and gradually die out towards the southwest, also following the trend of Pahau Torlesse basement rock exposure at the surface (with Quaternary marine and fluvial sediments dominating the southwestern geology). Figure 6b shows southerly dipping beds of the Kowai Formation (Pliocene) exposed in the sea cliff in the Glenafric field area, as well as a slight tilt to the southwest.

Very few studies have been done in this region; however, several marine terraces at Glenafric have been mapped (Yousif, 1987) and dated (Carr, 1970) based on geomorphological features. Previous work indicates that there are four terraces all Quaternary in age (Yousif, 1987), dating the most extensive terrace (shown in Figure 6a) between 60-80 ka (Yousif, 1987; Carr, 1970). Uplift rates and marine terrace deformation along the nearby Marlborough coast (north of Glenafric) from Cape Campbell to south of Kaikoura indicate that local structures have a large impact on uplift, specifically contractional fault/fold structures south of the Alpine Fault and its associated strike-slip faults (Ota, 1996).

Figure 6.) Field area overview. a (adjacent) This image shows a general overview of the study are with the most extensive terrace in the foreground and the Kate anticline tilting towards the southwest in the background. The view is from the northern edge of the MacIntosh Farm to looking southwest towards the Heard Farm (See Figure 7 for location). b) (bottom) An aerial photo of the coast near the Heard Farm. This image shows a southward tilt of the Kowai Formation, denoted by the blue and orange dashed lines. The blue line represents the unconformity and the orange lines represent bedding.

Methods

In order to determine the uplift rates along the Glenafric coast this study must assign ages and constrain marine terrace inner edges along the coastline of Glenafric. Essential data for determining inner edge elevations and uplift rate include: cross-sections of individual GPS surveys collected along a stretch of coast extending from Teviotdale to the landslide area north of Glenafric, topographic profiles created from LIDAR and 10m DEM data, marine terrace ages determined from optically stimulated luminescence (OSL) and amino acid rasterization (AAR) dating, and correlations between inner edge projections and their proximity to an anticline. The direction of fold propagation and anticlinal tilt will be considered throughout the study, especially in context of their effect on marine terrace uplift rate.

Constraining marine terrace elevations and therefore uplift rate is dependent on finding and estimating location and elevation of marine terrace inner edges. Elevation of the inner edge is a feature of eustatic sea level as well as vertical tectonic movement. The inner edge is the closest approximation to mean sea level, forming at the paleo seashore (Figure 7; Matsu'ura, 2013), thus providing a relatively easy landscape to identify in the field. Knowledge of past sea level elevations indicates the time of marine terrace formation, as marine terraces form at sea level highstands. This facilitates calculation of uplift rates and determination of deformation relative to anticlinal growth and southward propagation.

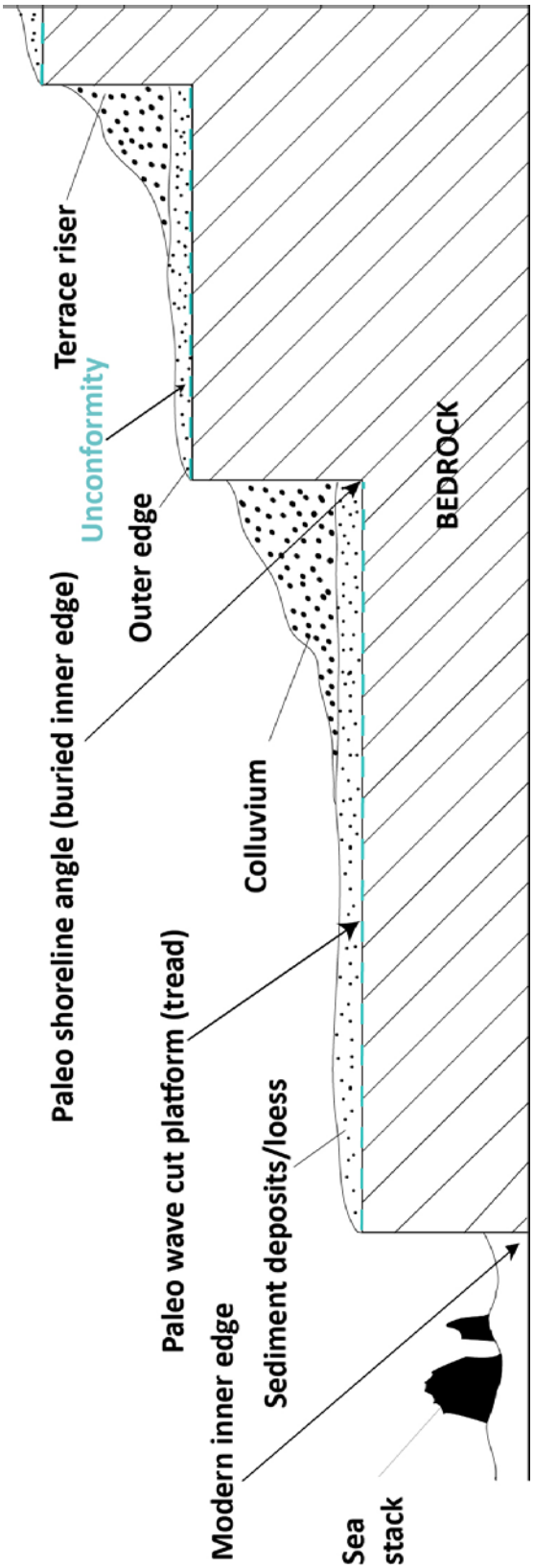

Figure 7. Schematic cross-section of a flight of marine terraces which provide a context for the methodology used in this study (from Gardner, 2012).

Because Glenafric has up to ~15m of loess, river alluvium, and marine sediment that bury the marine terrace inner edge, it is difficult to find and measure the exact elevation of the inner edge. Therefore, it is important to determine the elevation of the unconformity and project the slope into the paleo sea cliff to approximate the inner edge. In order to collect the most accurate data, five GPS surveys at different locations along Glenafric were conducted taking points at unconformities, terrace treads, risers, and inner edges (Figure 7). Inner edge locations were based on sedimentology (beach facies) and presence of an unconformity. Sediment indicative of beach gravel (well-rounded, well-sorted, course grained gravel) was a primary factor in determining whether a location was near an inner edge.

In the lab, an ArcGIS map including LIDAR (light detection and ranging), a 10m DEM, aerial photos, and geologic and topographic maps (Christchurch, Rangiora, Motunau Beach, Waipara, and Amberley Beach) were used to complete data analysis (Table 1). All 5 GPS surveys were plotted on the map. LIDAR and the geologic map (Figure 5) were used specifically to correlate terrace inner edges and distances to the Kate and Cass anticlines. LIDAR was also used as a method to measure elevations and topographic surveys away from GPS surveys to construct cross-sections for data analysis. Cross-sections were used for projecting inner edge estimations at the paleo-sea cliff, similar to the methods used by Matsu'ura (2013).

GIS Data Layer	Explanation
10m digital elevation model (DEM)	Three-dimensional representation of the Glenafric coast, which allows for elevation data collection and LIDAR use. Raster size of 10X10 cell. The DEM was obtained from the GNS website as part of the Qmap series.
250k topographic maps	1:250000 scale that includes UTM northing and easting coordinates. Data obtained from https://data.linz.govt.nz/
Georeferenced digital orthophoto quadrangles (DOQs)	Digital aerial photos with UTM easting and northing coordinates for each point on the image. Data obtained from https://data.linz.govt.nz/
Yousif Glenafric terrace tiff	Digitized map of Yousif's final geologic map outlining four flights of terraces. Used for comparison and starting point for GPS survey (Yousif, 1987).
LIDAR clip	Remote sensing technology that measures x, y, z coordinates. Elevation accurate to .09m. Used to construct topographic profiles. AAM Geoscan, a geo information solutions company, provided LIDAR data.
DGPS surveys	Each DGPS point has a specific location on the GIS map and exact coordinates can be found through the attribute table corresponding to each survey. Attributes include elevation, UTM coordinates, PDOP, and a description of the GPS location.
Geologic map (Qmap)	Digital map of the geology of the field area with a 1:250000 scale. Maps obtained from http://www.gns.cri.nz/

Table 1. List of GIS data layers and their purpose

Because not all GPS surveys were perpendicular to the coast, it was necessary to adjust and reposition the points perpendicular to the coast. This process involved sketching each GPS survey on a piece of graph paper and estimating approximate distances between points. A line perpendicular to the coast was drawn and each point was orthogonally projected to the new line (Figure 8). Using the 10m DEM and a ruler, ratios of the distances between each point on paper and the 10m DEM were calculated and plotted on a graph to create a cross-section. If points were too far away from the coast-perpendicular line, however, it could result in poorly constrained orthogonal projections. That is, points could be projected to locations ahead or behind structures and/or other GPS points that would distort the cross-sections and therefore inner edge projection. Therefore, fairly distant points were not included in the profiles/cross-sections.

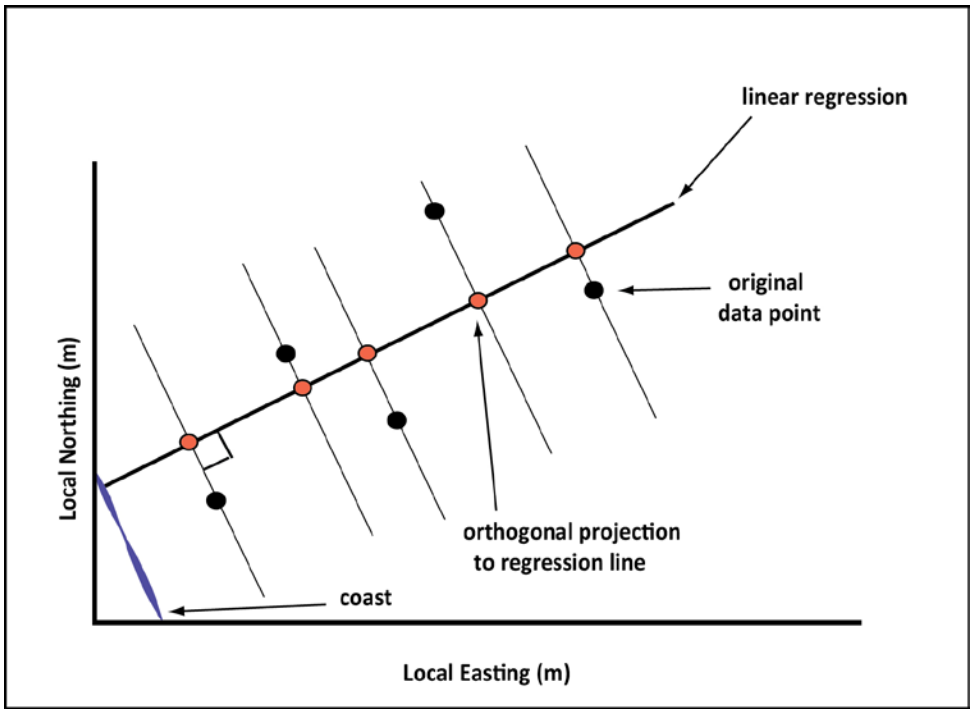

Figure 8. This figure depicts the general process involved in creating an orthogonal projection of the GPS survey points onto a cross-section. The blue amorphous line near the origin represents the coastline, the base for which all orthogonal projections were drawn parallel to. Reprinted from Trinity University student thesis: (Covault, Deformation along the margin of the North American plate in north central California between Alder Creek and Mendocino as recorded by Quaternary marine terraces, 2004).

Shell samples were collected at various locations along the coast for AAR dating by the Amino Acid Geochronology Lab at Northern Arizona University by Darrell Kaufman. The shells collected for this study were T. spissa fossils (Figure 9), an abundant fossil located throughout New Zealand. As different species have different rates of L/D conversion, it's important to use the same species for AAR analyses. AAR dating is based on the decomposition of the "L" amino acid configuration (the configuration associated with living organisms). Once an organism dies, the "L" amino acid gradually converts to a "D" amino acid, allowing scientists to use the D to L amino acid ratios to date the age of the organism's death (Bradley, 1999). Another dating method, optically stimulated luminescence dating (OSL), used in an ongoing related study through Penn State University, is used to constrain the age of marine terraces as well.

Figure 9. Image of the T. spissa shells collected from Glenafric, GPS 4.3. These shells were used for AAR dating.

Data and Results

Figure 10 shows the location of all GPS surveys and the general area of the three farms used for fieldwork. Black lines mark the location of topographic profiles useful for terrace correlations. GPS surveys trend primarily perpendicular to the coast and topographic profiles primarily parallel to the coast. GPS surveys were started at the coast and moved inland. Figure 10 was constructed using two GIS layers (Table 1), a series of Georeferenced DOQs and topographic maps.

Stratigraphy of Field Area

Each cross-section consists of up to ~15m of sediment burying marine terrace inner edges near the coast; and little to no sediment (due to erosion) more landward near the top of terrace flights. In general, most cross-sections, with the exception of cross-section 6, exhibit similar stratigraphy (Figure 11):

1. A basal erosional unconformity on ~30m of Kowai bedrock
2. A lower unconsolidated Quaternary sediment unit of well-rounded and well sorted cobble/pebble beds with cross-bedded and lenticular sands and locally abundant mollusks and gastropods. This unit generally grades seaward into bioturbated, wavy laminated fine sand and is 5+/- 3m thick.
3. A conformably overlying unconsolidated Quaternary sediment 6+/-3m thick consisting of alluvial/lacustrine sediments. Poorly sorted, matrix-rich, subangular sediments define this unit, ranging in size from pebble to fine sand. A muddy matrix is present in this unit at times. Bedding tends to be wavy and lenticular.

4. A massive loess deposit occasionally comprised of two distinct layers blankets most of the landscape. This layer is 6+/-3m thick.

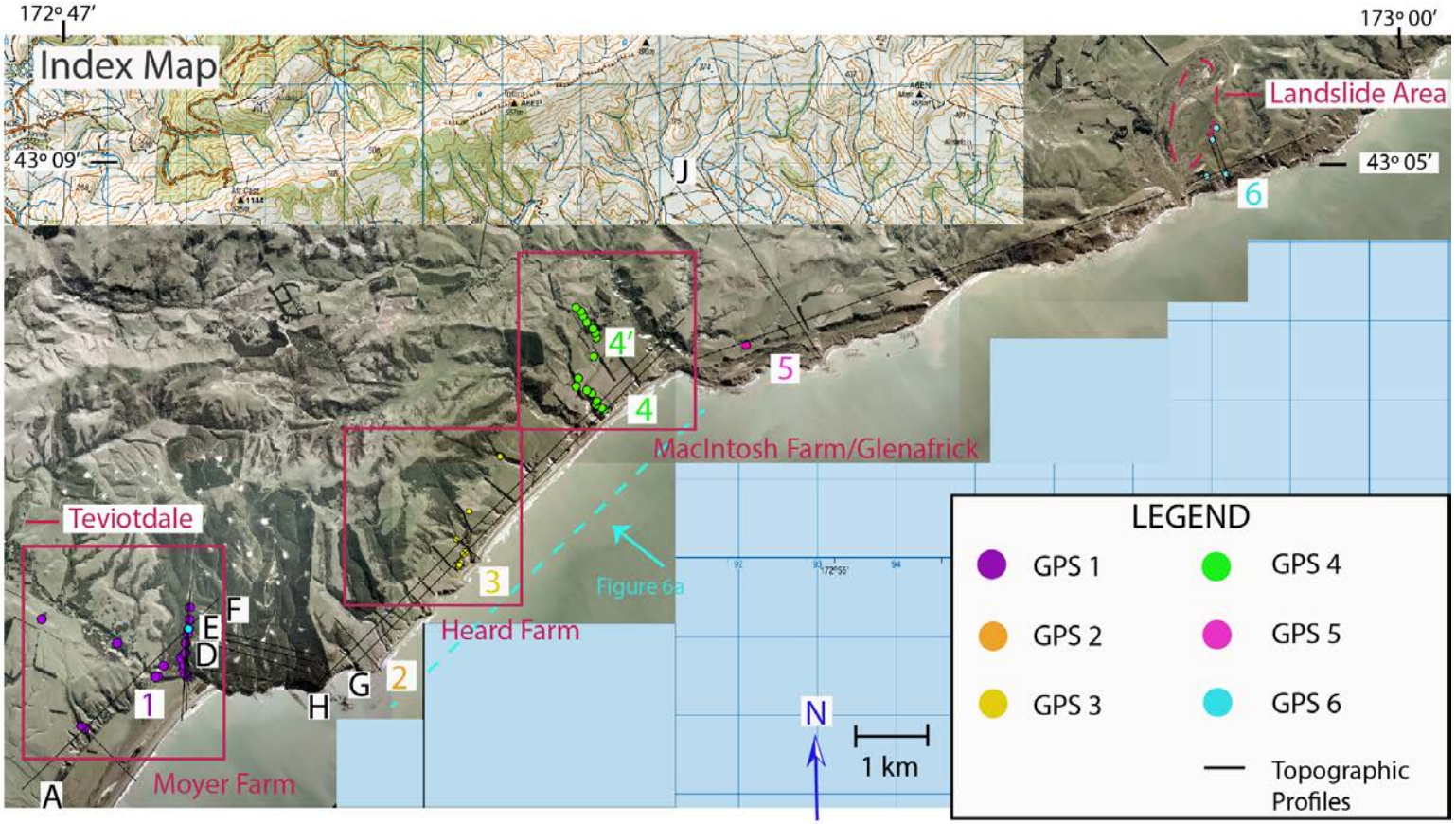

Figure 10. Index map showing the Glenafric study area. The area extends from Teviotdale in the south to the landslide area north of Glenafric. This map shows all GPS survey locations which are marked by colored circles corresponding to a colored number. The LIDAR profiles, marked by a solid black line and labeled with a letter (to the left of the line) serve as tools for terrace correlation. Some black lines are unlabeled as they are not specifically talked about in this study but were useful for data analysis. Red boxes indicate the general areas of specific field locations and will be referred to throughout the study. The section of the coast shown in Figure 6a is noted by the blue dashed line (Figure 2 for location).

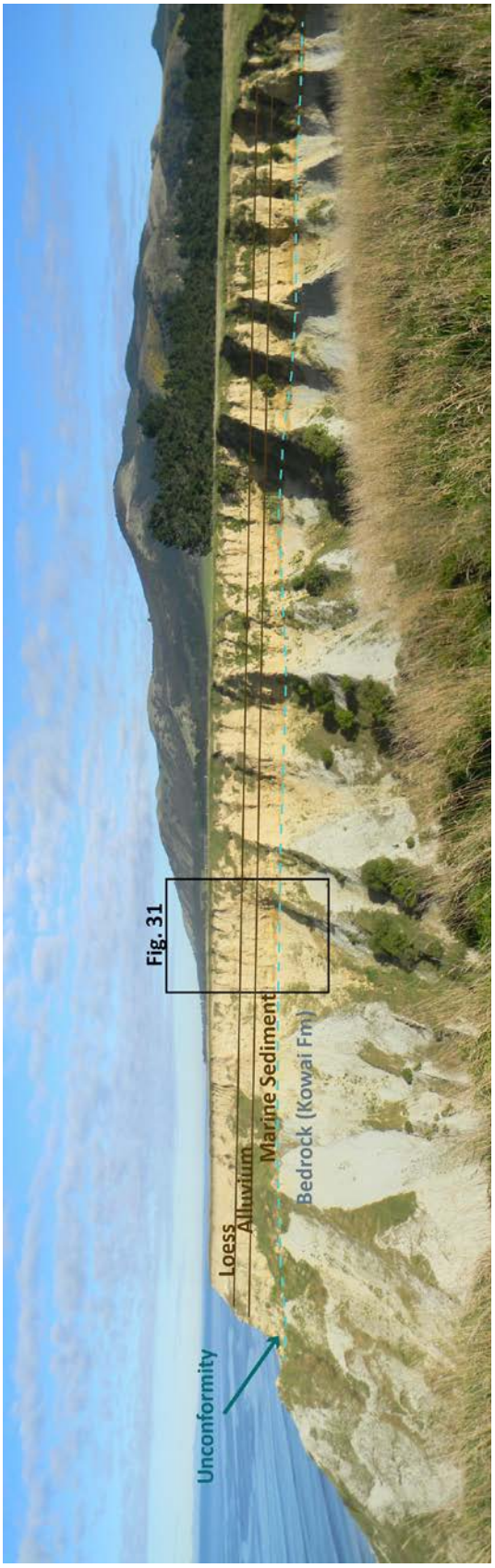

Figure 11. Marine terrace unconformity and overlying Quaternary sediments. Sediment cover is ~15m thick. This area is located at the most seaward end of GPS Survey 4 (See Figure 7 for location.)

Cross-Sections

Cross Section 1

Cross-section 1 is the southernmost survey along the Moyer Farm (See Figure 10 for location; Figure 12 for cross-section). Observations at GPS 1.8 suggest a marine terrace unconformity: well -rounded and sorted pea-size pebbles, imbricated pebbles, and wavy laminations (Figure 13). In particular, Figure 13a shows the wavy laminations that would only occur in shallow marine/beach environments. A close-up view of Figure 13a (Figure 13b) shows imbricated, well rounded gravel dipping seaward, indicating marine sediment. Gravel indicative of marine sediment is also present further south in survey 1 (Figure 14) at GPS 1.19, suggesting a possible marine unconformity.

Figure 12 shows varying unit thicknesses with a maximum marine sediment thickness of ~15m occurring at point 13. GPS 1.12-1.14 marked the tread of a possible terrace; however, the supposed tread did not maintain elevation consistency, dropping ~8m in elevation from GPS 1.13 to GPS 1.14. Confusion surrounds this particular area as rounded marine cobbles and interbedding was present at GPS 1.12 and 1.14, yet absent at GPS 1.13. Similar to GPS 1.12 and 1.14, GPS 1.15 showed signs of an unconformity with large rounded cobbles. Although an exact location was not assigned, it was assumed an inner edge existed in the region between GPS 1.12 and 1.15. GPS 1.1-1.7 and 1.19-1.21 are not plotted on the figure, as they could not be orthogonally projected.

Projected inner edges (Figure 12b) were estimated to be in close proximity to GPS 1.8 (~33+/-0.6m) and GPS 1.14 (~84+/-10.6m), both areas that provided evidence of inner edge marine sediment on the bedrock unconformity. The inner edge elevation projected through GPS 1.8 is ~ 33+/-7 m, and the inner edge elevation projected through GPS 1.14 was ~ 79+/-3m.

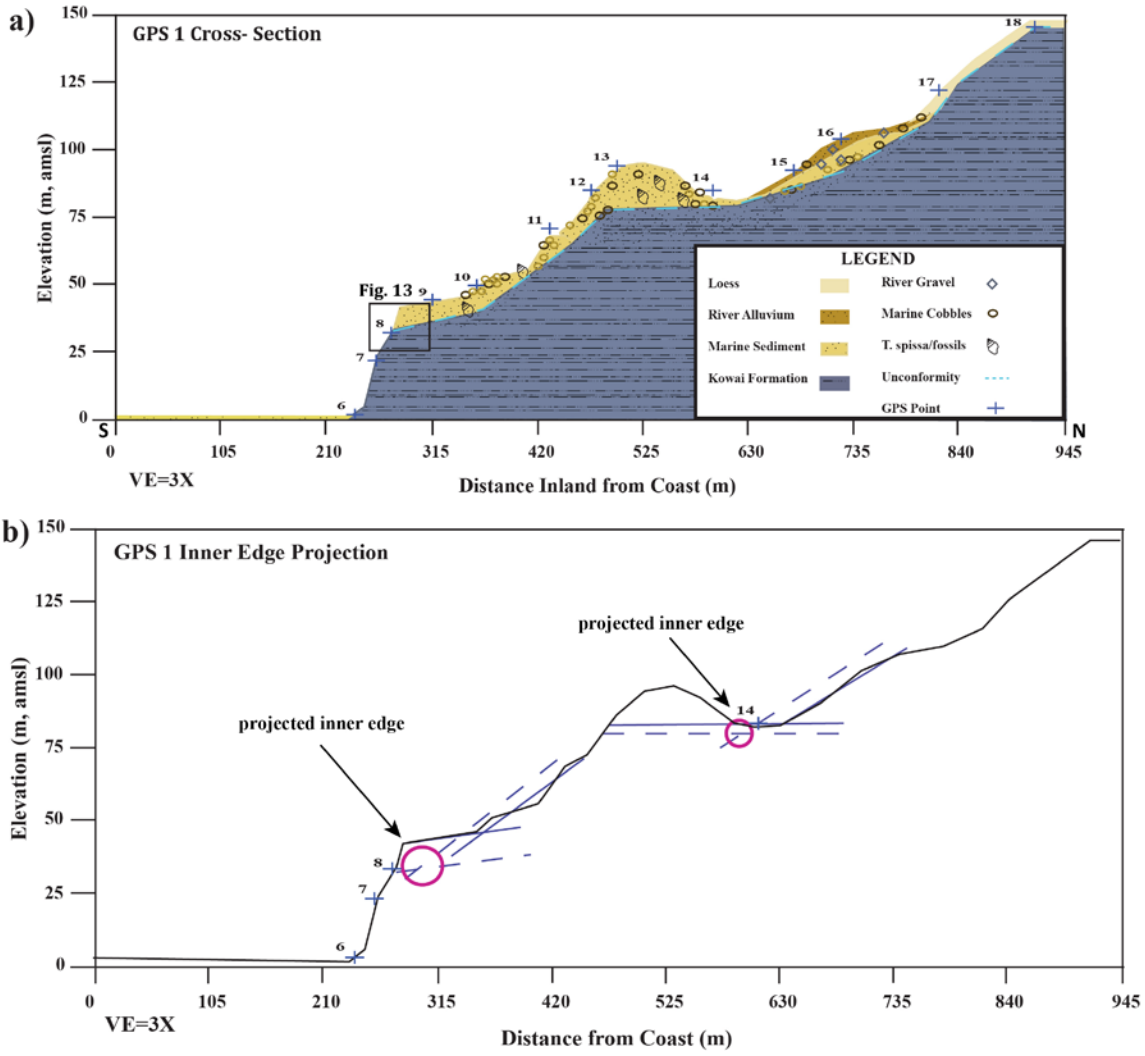

Figure 12. a) Cross-section of GPS survey 1 and stratigraphy overlying the unconformity. Survey 1 is located at the southernmost edge of the field area, south of the Heard Farm (See Figure 10 for location). The unconformity between the Kowai Formation and marine sediment is distinguished by a dashed aqua line. GPS 1.1-1.7 and 1.19-1.21 are not plotted on the figure. b) Inner edge estimations are circled in magenta in the topographic profile of the survey area. Estimations were based on proximity to the unconformity, presence of marine gravel, and proximity to topographic inner edge. The radius of the magenta circle represents the estimated margin of error with each projection. Bold dark blue lines represent the modern tread and seacliff. Dashed blue lines represent estimated unconformities and the paleo seacliff on which marine sediment was deposited. The point of intersection between the paleo seacliff and unconformity indicate the paleo inner edge (the magenta circles).

Figure 13. Inner edge indicators. a) This image shows the wavy laminations in the bedding of the well-sorted marine sediment. b) A close-up view of the marine sediment beds from the same outcrop as Figure13a more clearly shows the well-sorted and well-rounded nature of the laminated marine beds. All the pebbles imbricate seaward (blue lines indicate imbrication direction), verifying the sediment deposit as marine (See Figure 12 for location).

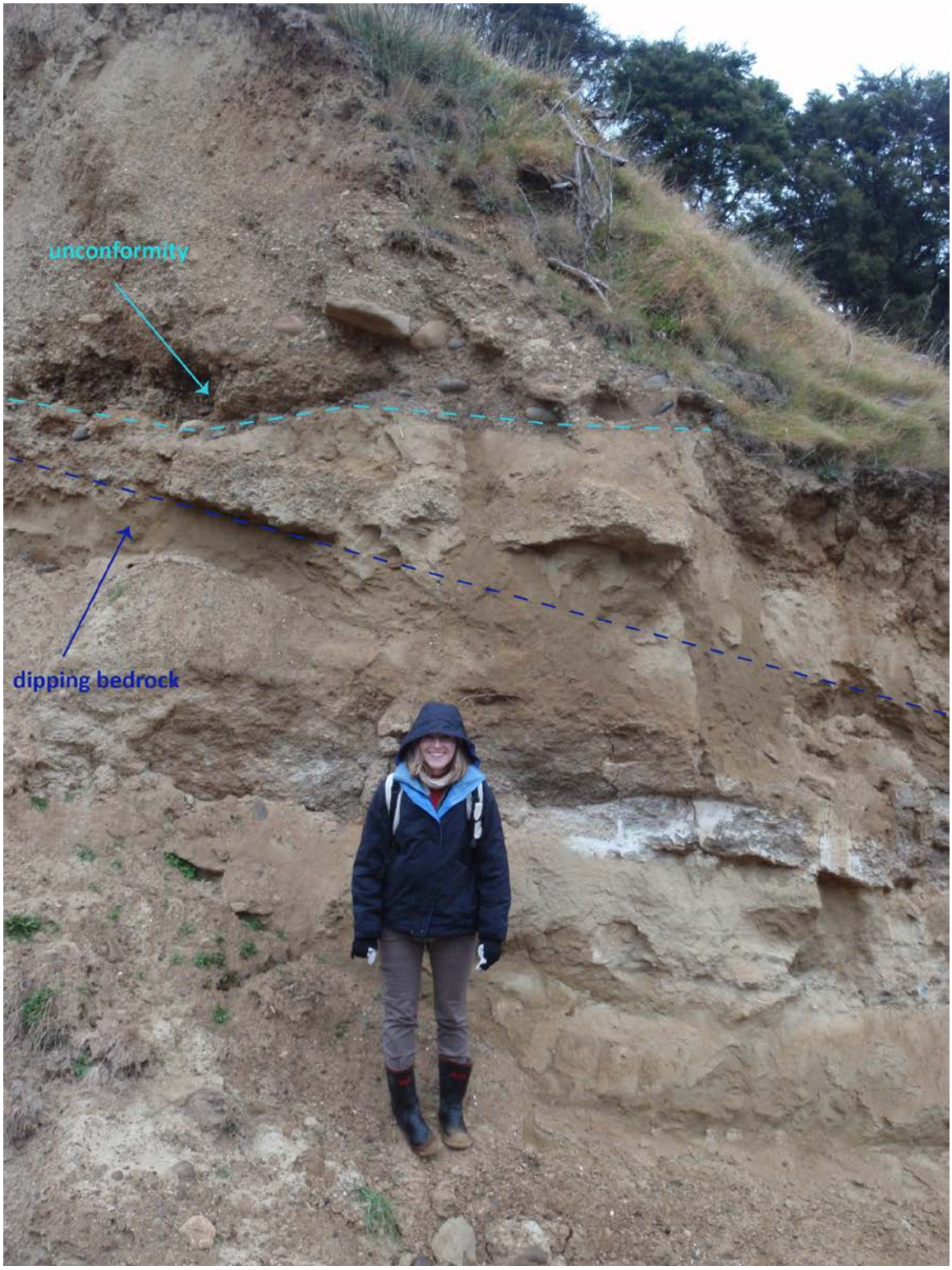

Figure 14. Marine gravel located above the unconformity (aqua dashed line) at GPS 1.19 (Mary Kate for scale). Kowai formation dips to the south similar to the Kate Anticline in Figure 6. The unconformity is located in the southern region of the Moyer Farm.

Cross-Section 2

Cross-section 2 (Figure 15) was created using LIDAR and the 10m DEM in ArcGIS because extreme flooding limited access in the field. The estimated thickness of each layer composing the sediment cover was determined using photos taken from an airplane of the coast (Figure 11). Loess and marine sediment were included in the cross-section because each was observed immediately south of GPS survey 1, an area in close proximity to cross-section 2. The loess and marine sediment thicknesses lie within the average thickness range of ~5-6m.

Figure 15a shows a possible inner edge location at around 350m landward of the coast, at an elevation of ~40m. Figure 15b shows a possible inner edge at ~60m, but Figure 15a shows that at around 350m inland, ~20m of sediment overlies the unconformity, projecting the inner edge closer to an elevation of 40m. This inner edge elevation is slightly higher than the inner edge elevation range for GPS 1.8 (33m+/-7; Figure 12).

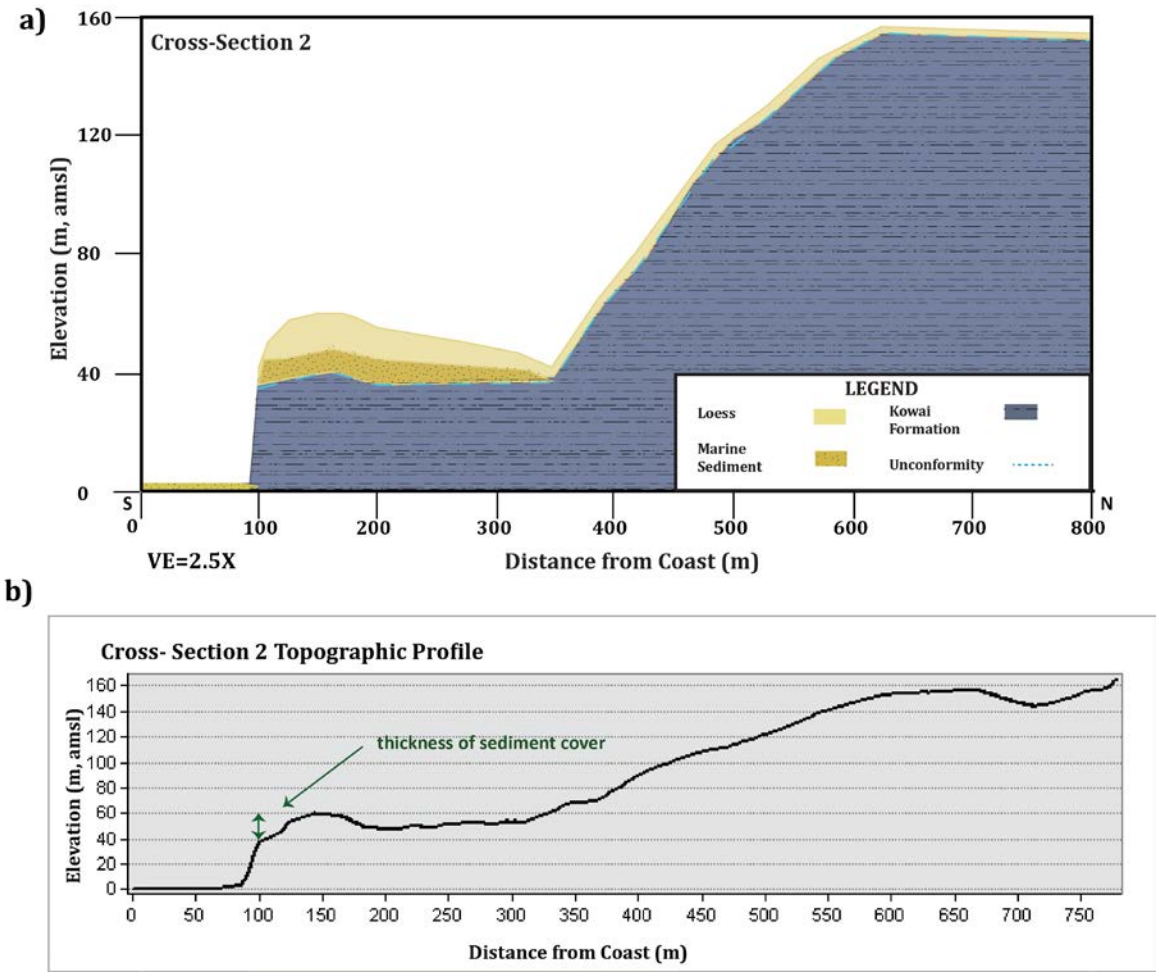

Figure 15. a) Cross-section of the area between the Moyer and Heard Farms (Figure 10 for location). A LIDAR topographic profile and the 10m DEM were used in construction of this cross-section because access could not be gained in the field. b) The topographic profile indicates an inner edge at ~40m elevation, covered by ~20m of sediment. Although this is an inner edge approximation, this inner edge elevation (40m) is similar to several other inner edge elevations (See Cross-section 1- Figure 12).

Cross Section 3

GPS Survey 3 (Figure 16) was conducted on the Heard farm (Figure 10). The topography of this survey exhibited a series of rolling hills overlying a dissected alluvial fan, as indicated by the thick loess deposits (~10m thick) observed throughout the survey. Figure 17 shows the stratigraphy and thickness of the loess deposits. Deposits were characterized by a layer of bedding separating two distinct loess layers composed of massive, well sorted silt.

GPS 3.6 (54+/-1.2m) is one of five points on the bedrock unconformity. GPS 3.6, however, exhibited rounded boulders at small knickpoints along the base of the creek bed, indicating a marine terrace inner edge. Marine shells (although not used to date the terraces) and bedrock were found along the slopes of the streambed walls as well, further indicating an inner edge. Projection of the inner edge placed its location landward of GPS 3.6 (Figure 16b) at an elevation of 53+/-8m.

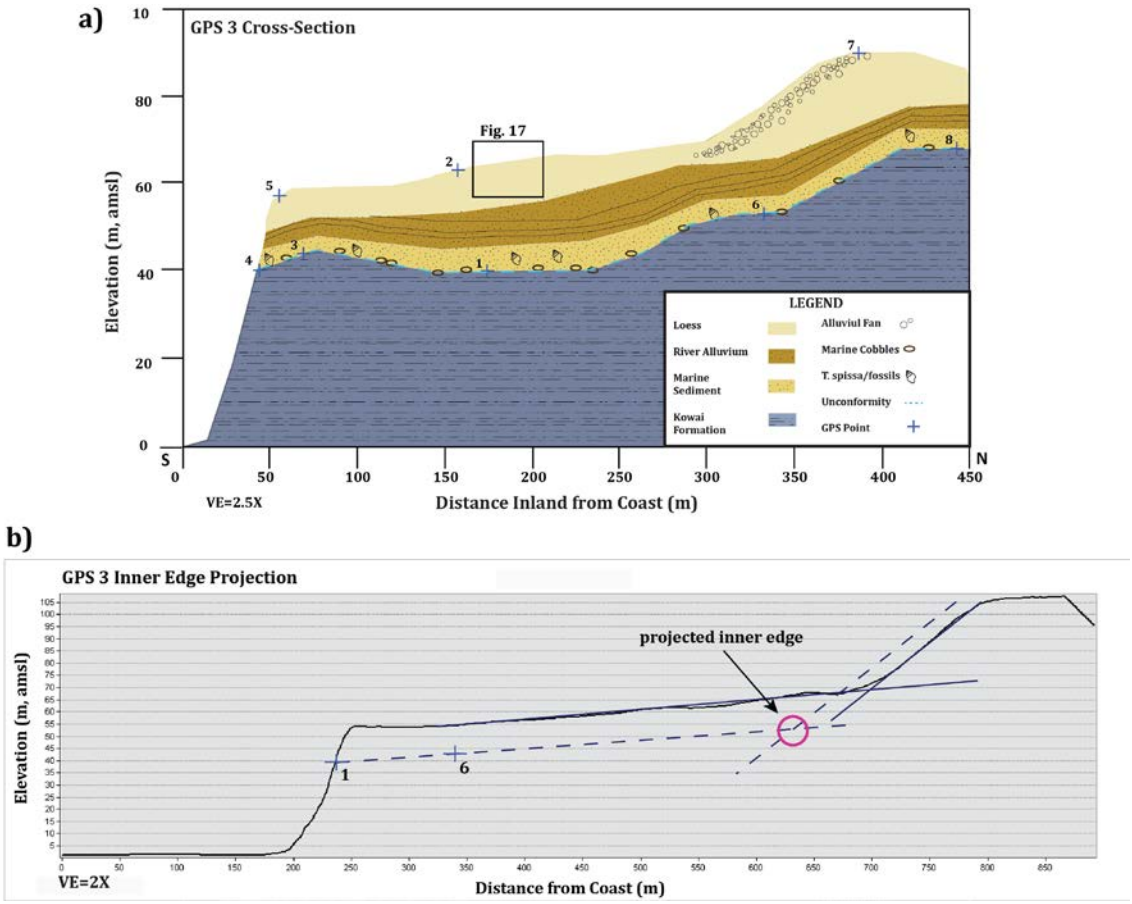

Figure 16. a) Cross-Section of GPS survey 3 conducted on the Heard Farm (Figure 10 for location). GPS 3.7 is located on top of an alluvial fan, represented by loess as well as alluvium. b) GPS 3.6 is the location estimated to be closest to the buried inner edge. The inner edge location was found in the stream bed adjacent to the stream knickpoint.

Figure 17. Massive loess deposits found in the same regions as GPS 3.2 (Tom for scale; Figure 16 for location). These loess layers are representative of the general loess deposits overlaying the river and marine sediment deposits. The loess layer is 5-7m thick and consists of two distinct deposits separated by the green dashed line.

Cross-Section 4

GPS survey 4 (Figure 18) was conducted on the MacIntosh farm (Glenafric). Survey 4 was broken up into 2 cross-sections (See Figure 10) based on the great length of the survey as well as its natural separation into two distinct survey areas, one farther south and closer to the coast (4) and the other farther north and more landward (4'). Two specific points stand out in this survey, GPS 4.3 and 4.7 as they provided shell samples for AAR analysis of marine terraces (sample locations shown in Figures 19 and 20).

Inner edge indicators were observed at GPS 4.7: a stream knickpoint, well-rounded and sorted marine cobbles that imbricate seaward, and T. spissa fossils. The elevation of GPS 4.7 was ~61 +/-4.5m. The inner edge projection (Figure 18c) for GPS survey 4 shows an elevation of 71+/-4m, only ~6m higher in elevation and ~200m inland of the field elevation. This inner edge projection is higher in elevation than the inner edge estimate of cross-section 3. Although no further evidence of an unconformity or marine sediment was found at higher elevations in the survey, several flat surfaces indicative of a terrace tread were located at ~120-125m and 194m respectively. Based on lack of marine sediment, it was assumed that bedrock was directly beneath the grass and was therefore not buried by sediment. Thus, the second projected inner edge (Figure 18cc) was projected directly on the surface of an assumed terrace tread at 123+/-3m.

The hypothesized highest tread (194m, GPS 4.16) occurs on the boundary of a drainage divide, making an inner edge calculation impossible.

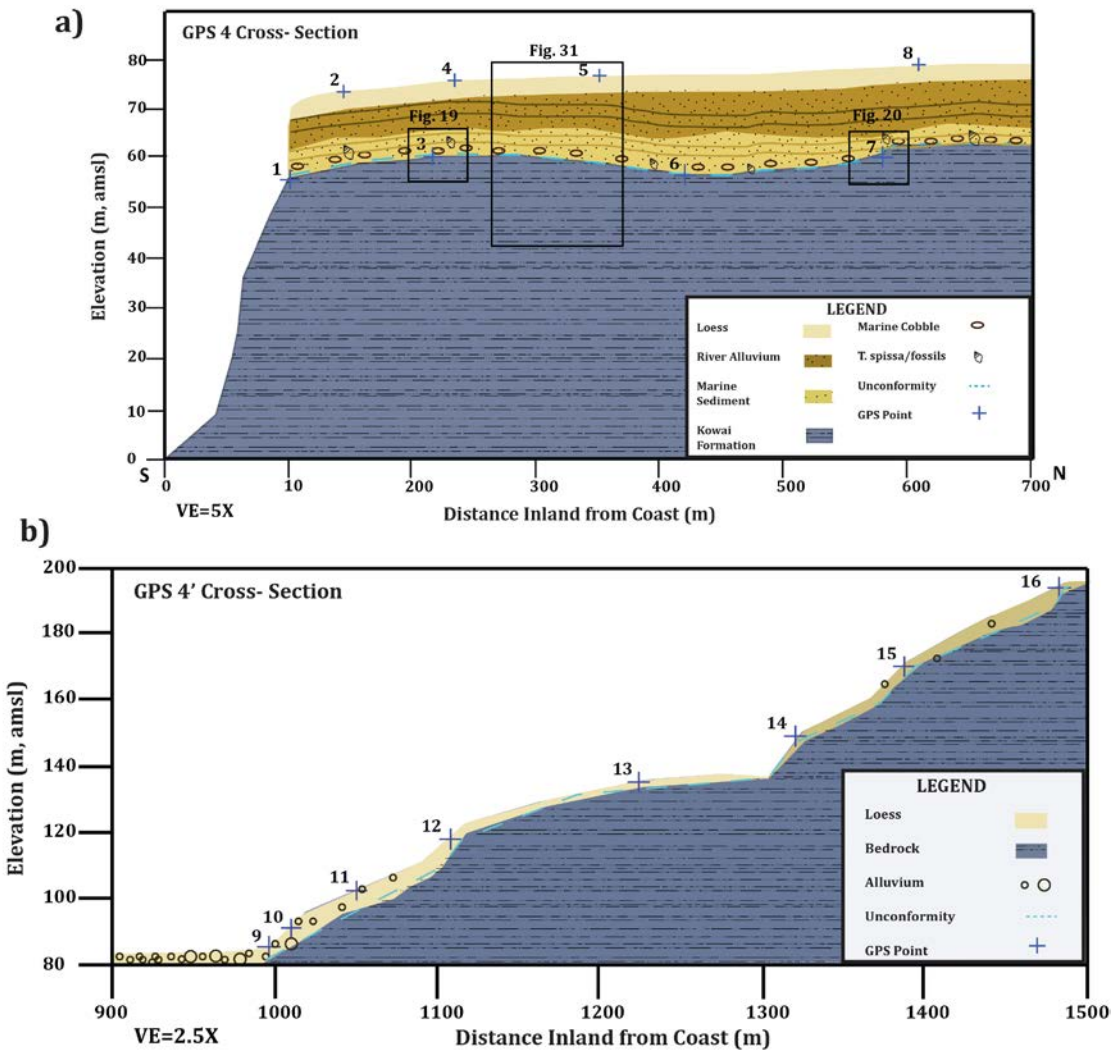

Figure 18. GPS survey 4 is divided into two separate cross-sections due to its exceptional length and break in line of section. All of the survey was conducted on the MacIntosh Farm (Figure 10 for location). a) The most seaward cross-section containing GPS 4.1-4.8. All samples used for AAR and OSL dating were collected near GPS 4.3 and 4.7. b) The inland cross-section containing GPS 4.9-4.16. Marine sediment indicative of an inner edge or unconformity becomes increasingly scarce as the survey goes inland, and therefore increasingly more bedrock is exposed at or near the surface.

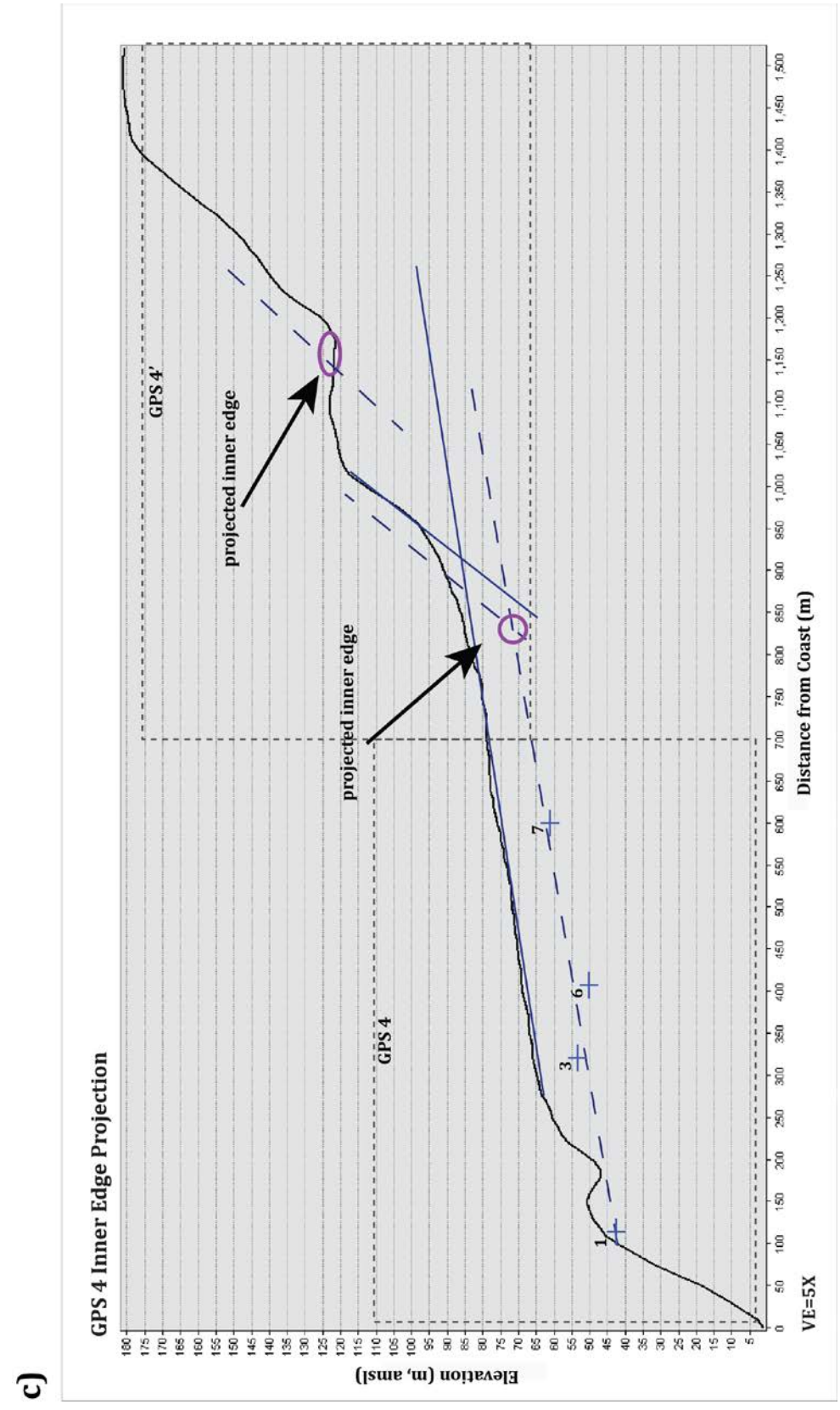

Figure 18. c) The two combined topographic profiles of survey 4. Each cross-sectional area is outlined by a black-dashed box. Two projected inner edges are estimated, one from GPS 1.7 and the other from GPS 1.13. Field evidence helped to indicate the general area of the inner edge around GPS 1.7; however, elevation was the primary factor for using GPS 1.13 as an inner edge as GPS 1.13 was a tread with little sediment separating the surface from the bedrock.

Figure 19. GPS 4.3 location serves as one of two primary locations for shell collection. As the image shows, all shells were collected along the unconformity boundary between the Kowai Formation (dark grey layer that shovel is on) and the marine sediment.

Figure 20. a) (top) GPS 4.7 at the inner edge, located at the base of a stream. Marine cobbles are observed seaward of the knickpoint, in the left-hand side of the image. b) (bottom) A close-up of the well-rounded and well-sorted marine cobbles from Figure 20a with a trowel for scale. The marine cobbles show seaward imbrication, much like the marine sediment from GPS survey 1.

Cross-Section 5

Unlike the other GPS surveys, survey 5 consisted of only one data point. A whole field day was dedicated to looking for evidence of a marine sediment unconformity or an inner edge and only one location was relevant. Similar to cross-section 2, construction of cross-section 5 (Figure 21) involved LIDAR and 10m DEM data as well as the limited field data. The survey consisted of following sporadic rounded cobbles along a stream north and inland, although no river sediment, marine sediment or fossils were found throughout the survey. GPS 5.1 was the location of a small, instream knickpoint and was the last place where rounded cobbles could be located in the field (Figure 22). It was unclear whether this point was indicative of a marine or fluvial unconformity.

The GPS 5 topographic profile (Figure 21b) offers little insight into the nature of the unconformity. The elevation for GPS 5.1 was 84+/-5 m, not falling near an inner edge, nor does it correlate to inner edge projections from any of the other GPS surveys. However, because GPS 5.1 presented a possible unconformity, it was plotted along the bedrock unconformity of cross-section 5 (Figure 21a).

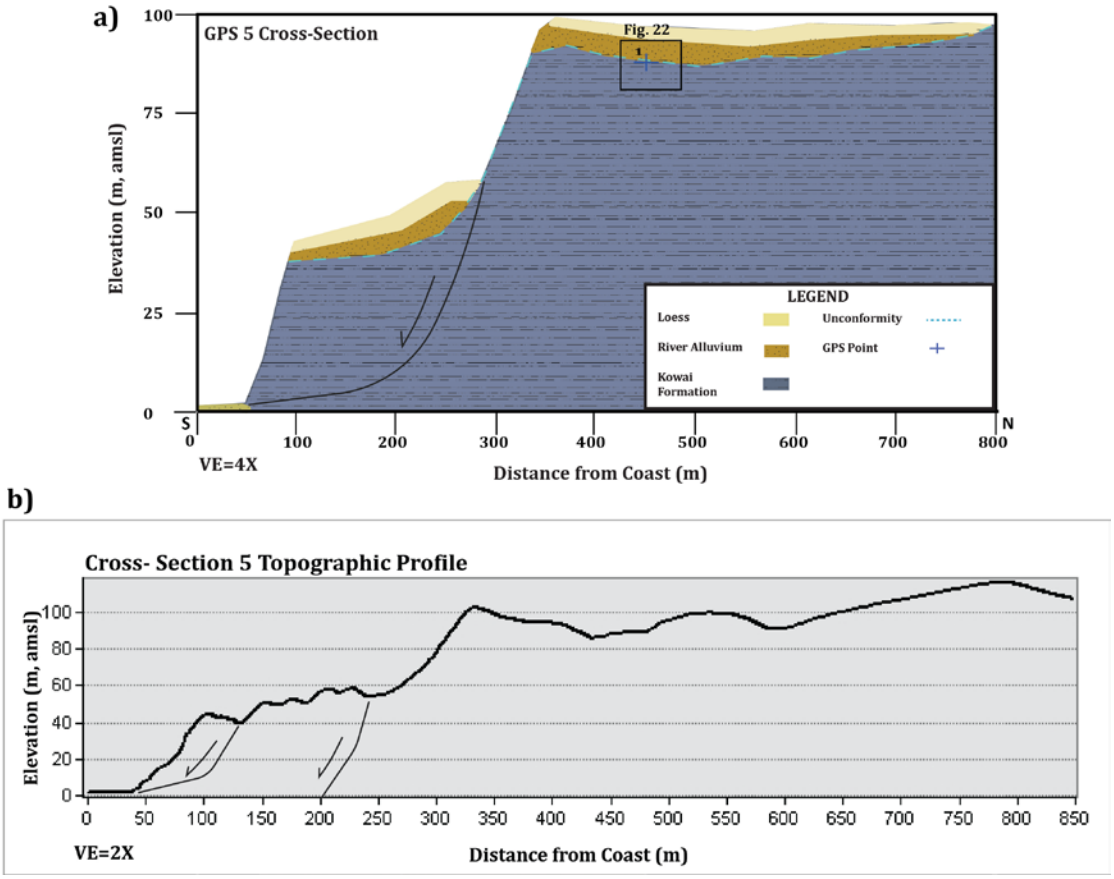

Figure 21. a) GPS survey 5 cross-section conducted north of Glenafric. The only point taken throughout the survey was taken at the last place where rounded boulders could be found along a stream. Rounded cobbles and boulders occurred intermittently along the stream; however, GPS 5.1 marked the end of any presence of cobbles and most likely indicated a possible erosional surface, if any. b) The topographic profile shows the landslide movement present along the sea cliff.

Figure 22. Image showing the last place rounded boulders were located. The boulders are circled in white.

Cross-Section 6

GPS survey 6 (Figure 23) was conducted in the northernmost region of the field area in the landslide area. Two GPS points indicated signs of an unconformity (Figure 24). Marine sediment and rounded cobbles were located at GPS 6.1. However this point was most likely not the site of original deposition because the cobbles directly overlie the boundary between colluviated sediment and disrupted Omihi Limestone (Figure 24). However, the presence of rounded cobbles did indicate proximity to an inner edge.

Inner edge indicators, however, were observed at GPS 6.2. The point was taken on the top a knickpoint with a direct view of emplaced marine cobbles. Unlike the two bedrock formations beneath the knickpoint, the overlying sediment layers were perfectly horizontal. The inner edge projection for GPS 6.2 was 110m, ~40m higher in elevation than GPS 4.7 from Cross-Section 4 (~70m). Similarly, GPS 6.4 (198m) was higher in elevation than GPS 4.16 (194m). Points from GPS survey 6 provided significantly to moderately higher inner edge elevations compared to other GPS surveys conducted in the Glenafric field area.

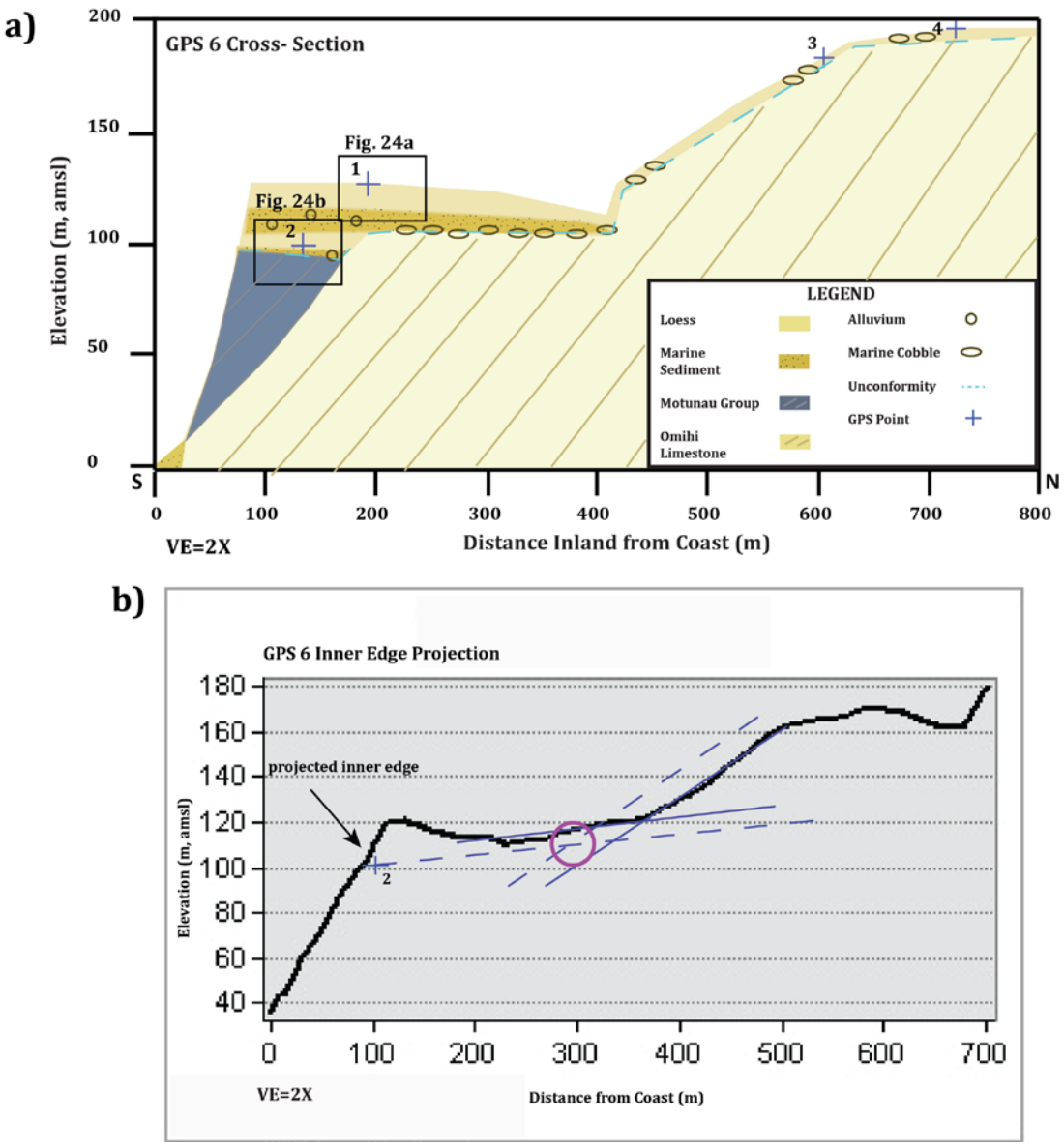

Figure 23. a) GPS survey 4 was conducted in the landslide area in the northernmost region of the field area. Two bedrock formations are present in this survey along the sea cliff: the Motunau Group and the Omihi Limestone. b) The topographic profile of survey 6 shows a projected inner edge elevation near the middle of the terrace tread. Evidence for an inner edge was present at GPS 6.2 indicated by a knickpoint and embedded marine cobbles along the elevation at the top of the knickpoint.

Figure 24. Field evidence indicating a possible erosional surface and inner edge (See Figure 23 for location). Unconformity boundary between the marine sediment and the Omihi Limestone at GPS 6.1. The rounded boulders are colluviated and most likely originated from a higher elevation.

Terrace Correlation

Topographic Profiles

Figures 25-27 show topographic profiles in the Glenafric area that lie perpendicular and parallel to the coast. These topographic profiles were created using LIDAR and the 10m DEM in ArcGIS. The purpose of these profiles was to obtain additional topographic information that could potentially augment GPS survey elevations and facilitate correlation of marine terraces.

Profiles G and H (Figure 25) show an apparent tilt towards the southwest. Topographic profiles G and H, parallel with the coast, show an elevation of ~80m in the north decreasing to an elevation of ~60m in the south. Not all topographic profiles show the southwestward tilt, however. Topographic profiles D-F (Figure 26), closely spaced at the southern end of the field area north of the Moyer Farm and parallel to the coast, exhibit a relatively constant elevation of around 100-110m. These profiles provide strong evidence of a flat surface at ~100m, an elevation higher than the flat surface elevation of GPS 1.14 (~80m). Comparison of the flat surface from the topographic profiles and the flat surface of GPS 1.14 shows a southwestward decrease in terrace elevation, similar to that of profiles G and H

Topographic profile A (Figure 27), passing through GPS survey 1, does not show an apparent tilt. However, it does show that previously mentioned GPS survey 1 outliers are consistent with GPS 1.8 which lies on the unconformity of the lowest marine terrace (Figure 12). GPS 1.3 and GPS 1.5, ~0.5 km southwest of GPS 1.8, lie on the unconformity at ~33m directly underneath the terrace tread. These elevations are in range with the inner edge elevation (33+/-7m). GPS 1.19 lies on

the terrace tread, but at a higher elevation of ~42 +/-9m, similar to GPS 1.9 at 45m on the same terrace tread (See Figure 11 for GPS 1.9 location). Topographic profile J (Figure 26) shows a profile similar to the orthogonal profile of GPS survey 5 (Figure 20-b). Profile J shows a flat tread at ~100m at 200m inland and Cross-Section 5 (Figure 20-a) shows a possible terrace tread at ~100m at 300m inland. Topographic profile J indicates that GPS 5.1 is more than likely indicative of a marine unconformity.

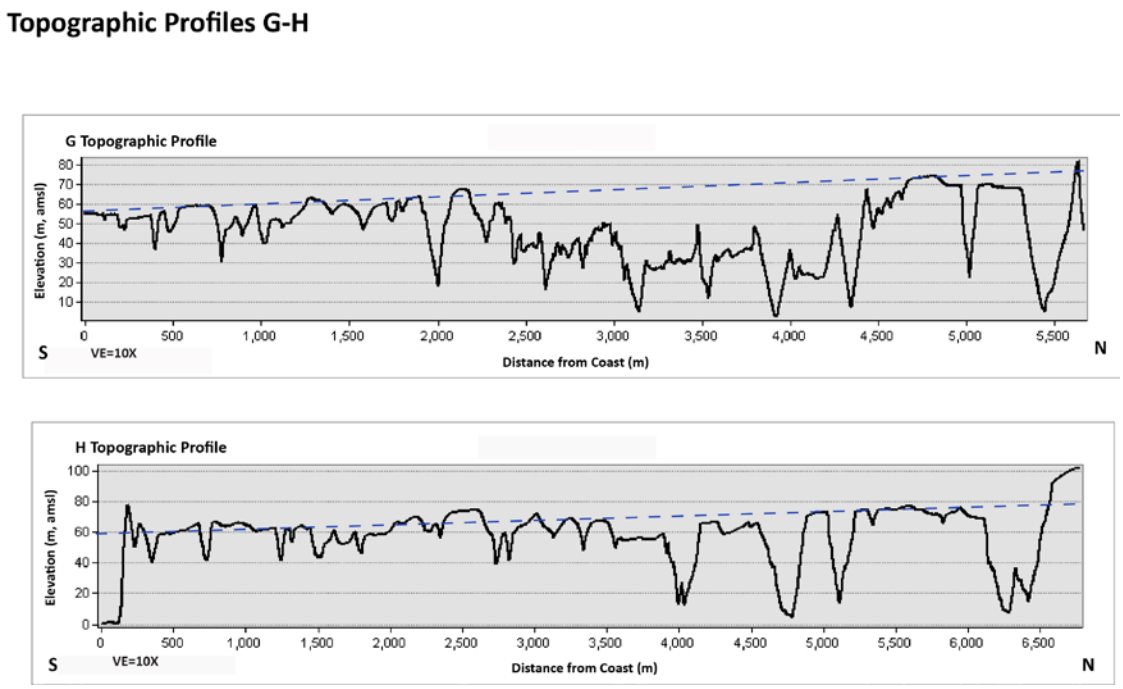

Figure 25. Topographic profiles G and H extend from south of the Heard Farm to the MacIntosh Farm. These profiles show a general southwest tilt as evidenced by the decrease in elevation from the northeast to the southwest (See Figure 10 for location).

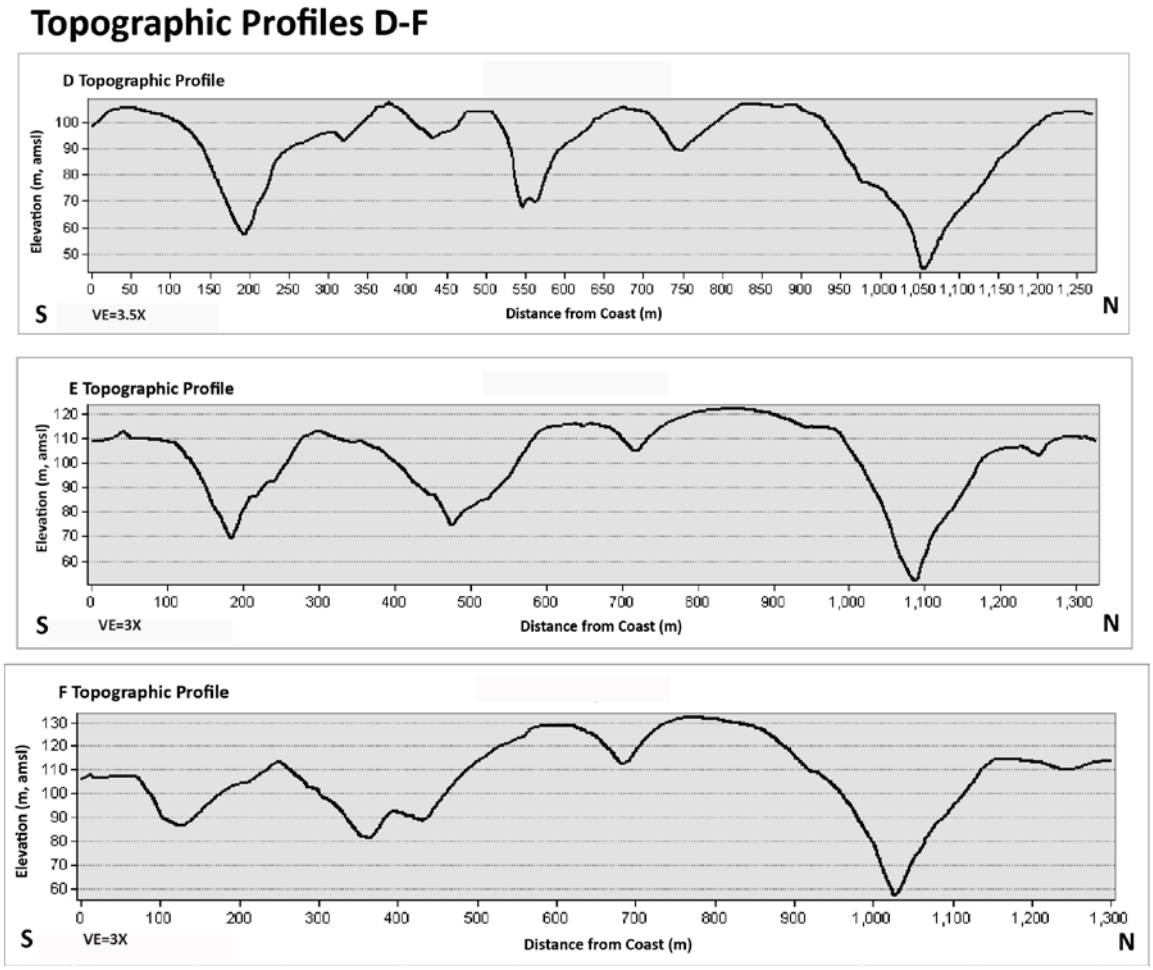

Figure 26: Topographic profiles D-F run parallel to the coast between the Moyer and Heard Farms. All profiles exhibit a relatively constant elevation at ~100m. These profiles do not exhibit a southwestward tilt as seen in profiles G and H (See Figure 10 for location).

Topographic Profile A

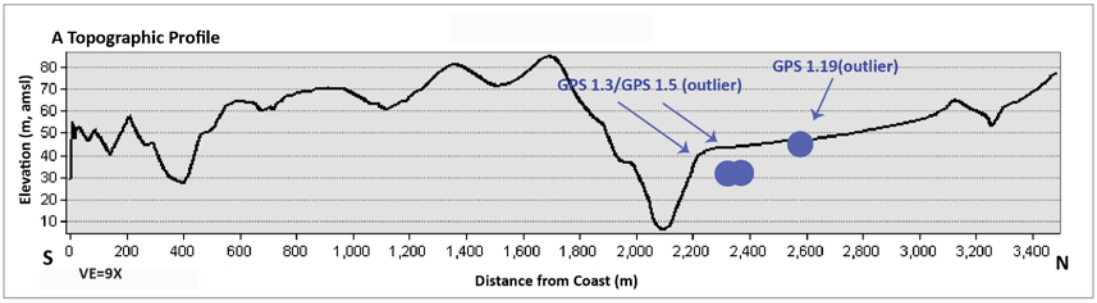

Topographic Profile J

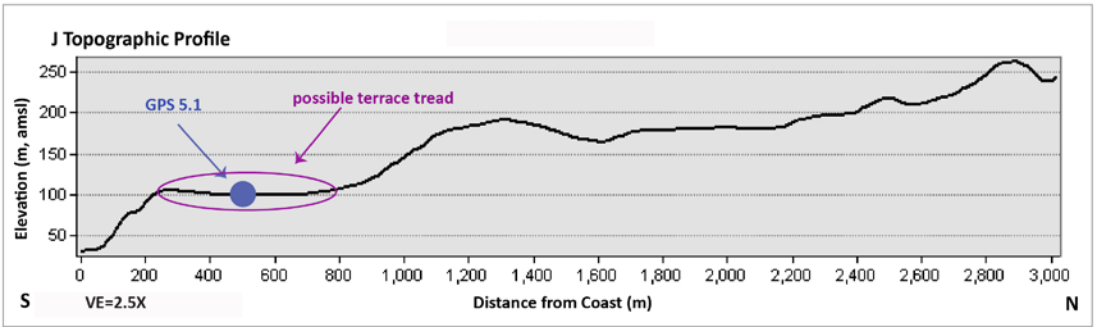

Figure 27. Topographic profiles A and J are located on opposite sides of the field area, A in the southern tip and J north of the MacIntosh Farm. Profile A serves as a comparison to the GPS survey data collected for survey 1. Several elevations, GPS 1.3, 1.5 and 1.19, can be plotted along the unconformity and terrace tread indicating consistency with GPS survey 1. Profile J proves that GPS 5.1 is more than likely indicative of a marine unconformity as GPS 5.1 lies directly on the tread and exhibits a similar elevation, ~100m, to the profile J tread (See Figure 10 for location).

Correlation of Terrace Inner Edges

Three marine terraces were identified and mapped (Figure 28) using the cross-sections and topographic profiles described earlier. Terrace elevations were then compared to the two closest fault-propagation folds within the Glenafric field area, the Kate, Cass, and Montserrat anticlines. Measurements were based on distance from the fold axis. Although the Kate anticline is a much smaller structure than the Cass and Montserrat anticlines, it is believed that Kate anticlinal growth will most significantly affect terrace elevation and uplift rate because it is closest distance to the flight of three marine terraces.

Terraces of similar elevations were grouped together; Qt_3 elevations range from ~30-100m; Qt_2 range from ~84-119m; and Qt_1 range from ~193-198m. Although there is a large range in elevations for each terrace, especially Qt_3, the elevations make more sense when compared to distance along the coast and proximity to the Kate and Cass and Montserrat anticlines. Field defined inner edges and points indicative of a possible erosional marine surface were plotted, correlated, and measured from all three anticlinal axes (Figure 29).

Figure 29a shows the distance of the inner edges and erosional surfaces to the Kate anticline axis, the local geologic structure hypothesized to be the primary influence on terrace uplift in Glenafric because it's closest to the marine terraces. GPS 6.2 and 6.4 were not measured to the Kate anticline because it does not extend that far north. GPS 1.8 and GPS 2 are closer to the Kate anticline than GPS 3.6, yet have a lower elevation meaning that proximity to the Kate anticline doesn't explain

all changes in elevation. Despite this discrepancy, all terraces show a systemic decrease in elevation to the south.

Figure 29b shows the distance of the inner edges and erosional surfaces to the Cass and Montserrat anticlinal axes, anticlines west of the Kate anticline. In general, the closer in proximity to the Cass and Montserrat anticlines, the higher the inner edge or erosional surface elevation, except at the very southern end of the field area near Teviotdale. GPS 4.16 (194+/-3m) and GPS 6.4 (198+/-3.3m) from Qt_1 as well as GPS 5 (84+/-5m) and GPS 6.2 (110+/-10m) from Qt_3 are all less than 4 km away from the anticlinal axis and exhibit a high elevation. In contrast, GPS 1.14 (79+/-3m) and GPS 4.13 (123+/-3m) from Qt_2 and GPS 1.5 (32+/-0.1m) and 1.3 (32+/-0.2m) from Qt_3 are 3.8km away from the Cass anticline axis, yet have the lowest elevations. Figure 30 shows a plot of uplift rate versus distance from the Cass Anticline. Although the coefficient of determination (R^2) is a small value the linear regression shows that as the distance from the Cass Anticline increases, the uplift rate decreases. This plot shows that anticlinal growth does not have a major impact on marine terrace uplift rate, but it does exhibit some influence.

Figure 28 shows that the points with the highest elevations (GPS 5 and GPS 4.16) either belong to the oldest terrace (like GPS 6.2 and 6.4) or are closest to the structural culmination, the structurally deepest rocks exposed in the anticline. The Pahua Torlesse (in grey), the oldest formation in the NCFTB, is located at the structural culmination and therefore must indicate the location that has experienced the greatest amount of uplift in response to the largest amount of slip on local thrust faults. Figure 28 also shows that not only the Cass anticline, but one of the thrust

faults responsible for anticlinal growth, the Hamilton Fault, tilt to the southwest under Quaternary alluvium (Figure 2). This structural culmination and southwest tilt indicate that proximity to an anticline is not the sole factor in terrace uplift, but terrace age and proximity to the structural culmination must be accounted for as well.

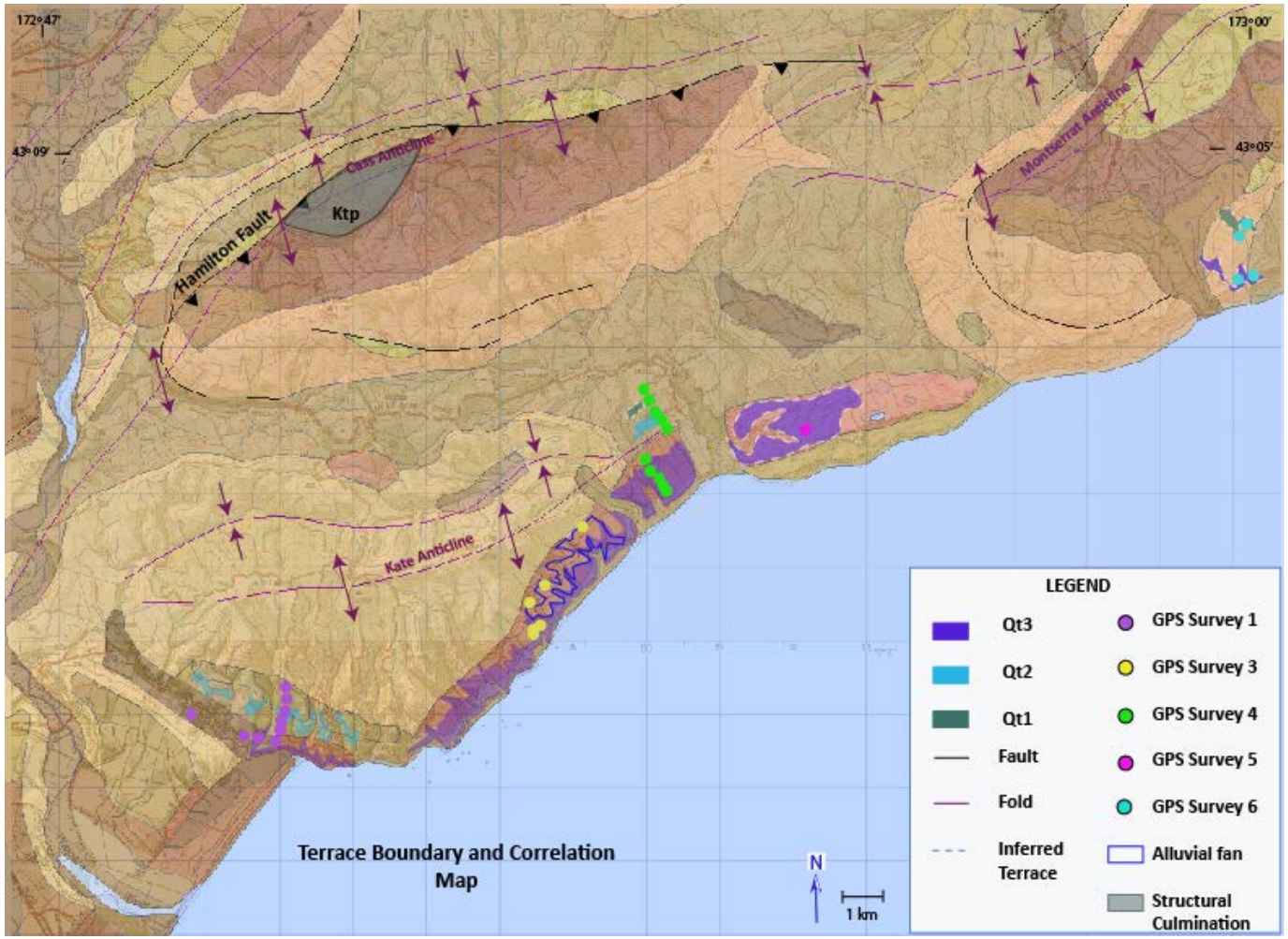

Figure 28. All GPS survey and relevant faults and folds are plotted on the terrace map. Three terraces were determined from field evidence and LIDAR extrapolation. Inner edge elevations were the primary source indicating terrace boundaries. Inferred terraces, terraces that could not be supported by substantial field evidence, are indicated by a dashed line. The alluvial fan from GPS survey 3 (Figure 16) is outlined by a blue line. The structural culmination is highlighted in grey and labeled as "Ktp."

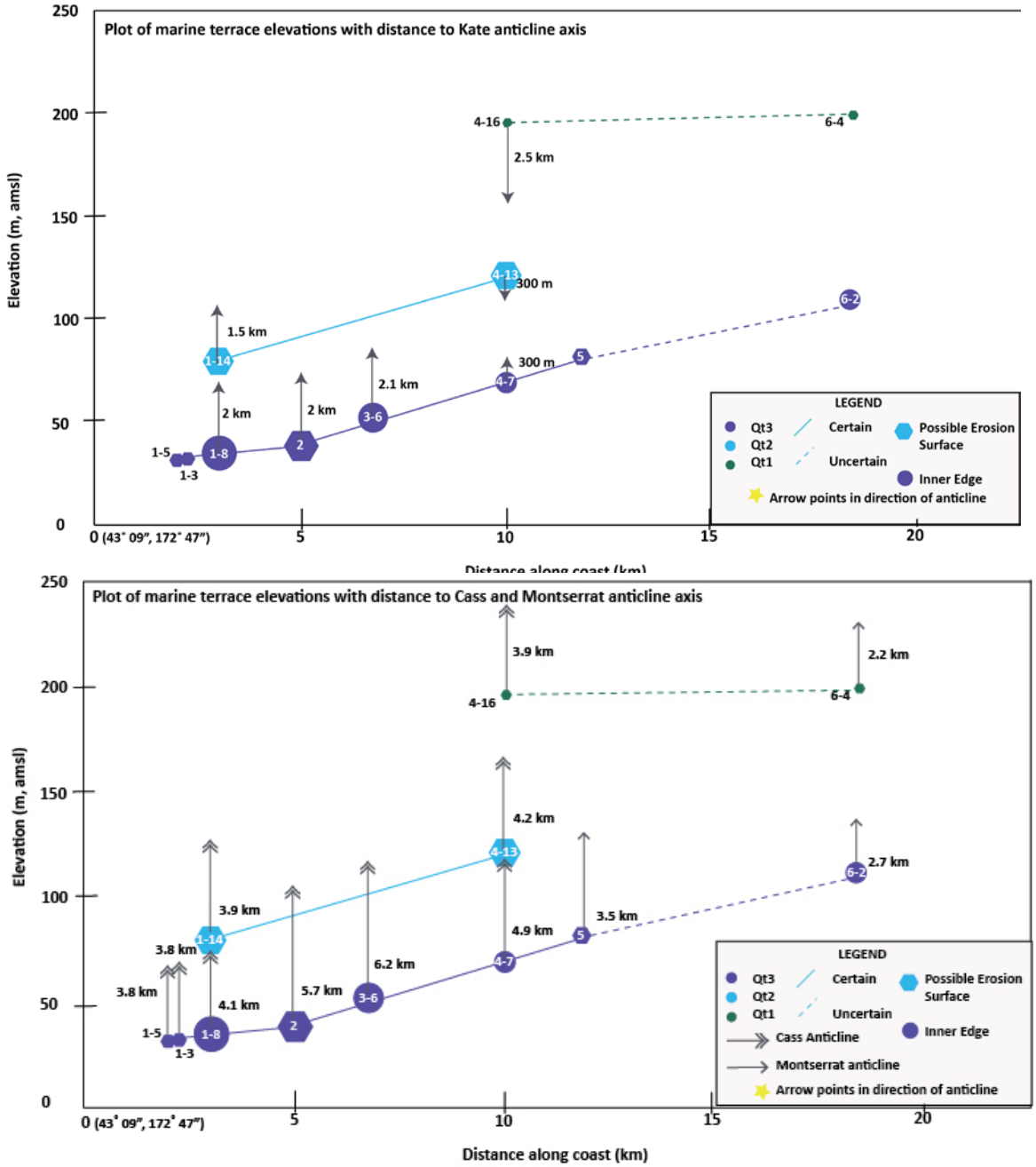

Figure 29. Terrace inner edges and unconformities are plotted with respect to distance to the axes of two local anticlines. a) Terraces are plotted against the Kate anticline based on distance along the coast and proximity to the anticlinal axis. In general, the closer to the anticline, the greater amount of uplift. b) Terraces are plotted against the Cass anticline based on distance along the coast and proximity to the anticlinal axis. In general, higher elevations are closer to the anticlinal axis, with the exceptions of GPS 1.5, 1.3 and 1.8.

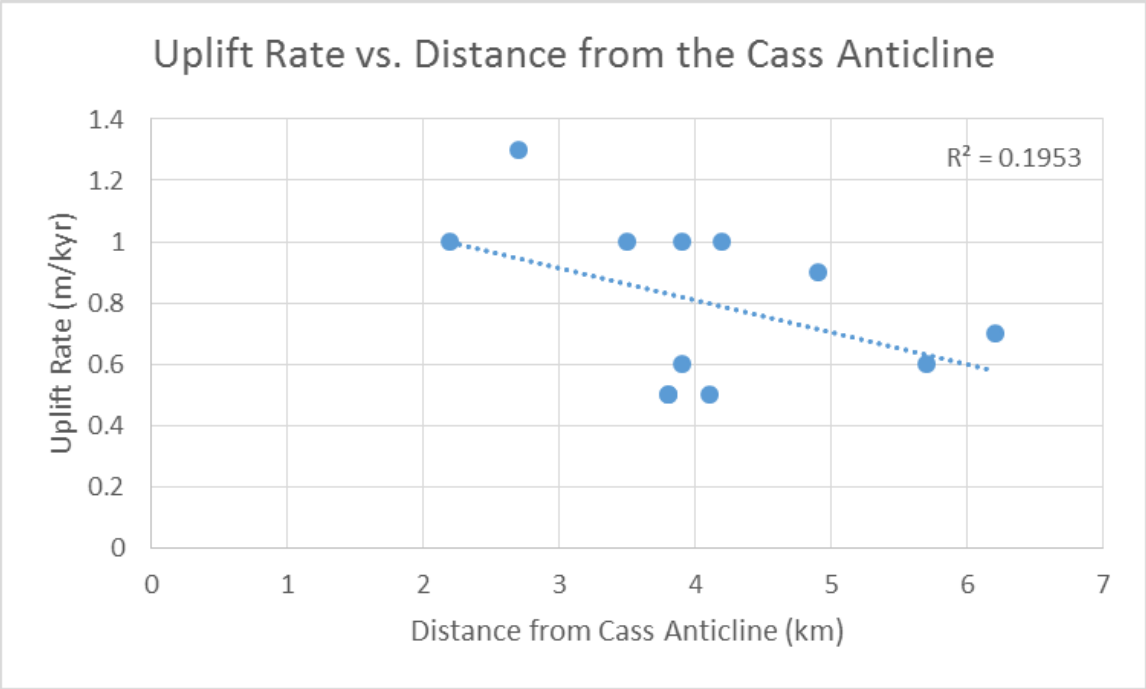

Figure 30. Plot of uplift rate versus distance from the Cass Anticline. The coefficient of determination (R^2) indicates a weak correlation between the two variables; however the linear regression indicates a positive correlation. The slope of the line shows that with distance from the Cass anticline, the uplift rate decreases. This signifies that fold growth has a minor influence on overall marine terrace uplift rate.

Terrace Ages and Chronology

All AAR and OSL samples relevant to this study are shown in Figure 29. All AAR samples from this study and one OSL sample from a concurrent study (highlighted in green in Table 2) were found in the marine sediment layer; and one OSL sample from the same concurrent study came from the river alluvium. T. spissa molluscs were used to constrain the ages of the marine terraces. Although many samples were collected throughout the field area, only a few samples from two locations, (GPS 4.3 and 4.7) were used for AAR dating (Table 2) as several field sites did not have T.spissa molluscs or the fragments collected were too small for dating.

Three different amino acid ratios (Asp, Glu, Ile) were used to constrain an approximate age for the AAR samples (pers. comm. Darrell Kaufman at Northern Arizona University). Two of the samples were taken from this study GPS 4.7 and GPS 4.3, and one from a concurrent study at Penn State, MAC-3. Two of the three samples, GPS 4.3 and MAC-3, were dated at around the same age (92 and 97 ka respectively) and grouped into the same MIS sea level, 5c at 96 ka. GPS 4.7 was slightly younger than the other two samples at an average age of 80 ka years. This sample was grouped in marine isotope stage (MIS) sea level 5a. This discrepancy is believed to be due to anomalous DL Asp values (see Table 2) for GPS 4.7 as GPS 4.3 and MAC-3 are 10+/-5 ka older than GPS 4.7, although both samples were collected seaward of sample GPS4.7 and all three samples are on the same terrace, Qt_3. Furthermore, GPS 4.7 was the first point in survey 4 to indicate an inner edge and must be older than the points sampled seaward of this point. It would be quite

difficult to get a 5a deposit landward of the 5c deposits on the same terrace without any evidence of a 5a deposit at the seaward 5c locations.

The alluvium sample dated using OSL, OSL-MAC, (Table 2) was also found on the MacIntosh farm (Table 2) near samples GPS 4.3 and MAC-3. The sample was dated at 98.7 +/_ 4.7 ka, slightly older than samples MAC-3 and GPS 4.3. This means that the OSL sample falls in MIS 5c sea level, proving that sample GPS 4.7 is most likely an outlier. The marine sediment sample, OSL-Glenafric, was found just above the bedrock unconformity. Although marine sediment is exposed to sunlight like river sediment, sample OSL-Glenafric was dated at >231.4+/-13.9 ka, significantly older than the other samples. Lack of exposure to sunlight was most likely the cause for this outlier. Therefore, sample OSL- MAC was used for terrace correlation and dating. In conclusion, relevant ages constrain marine terrace Qt_3 to MIS 5c.

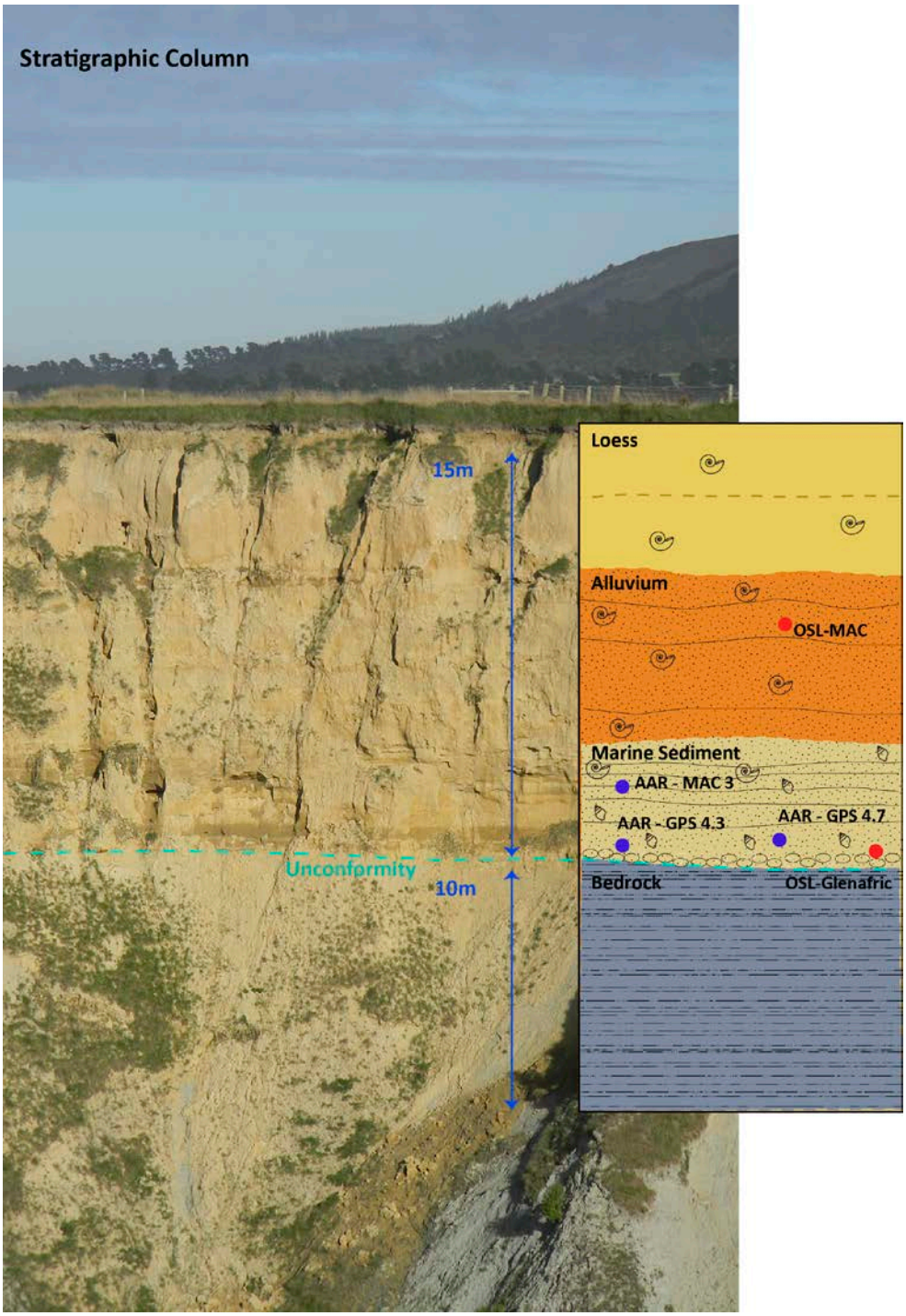

Figure 31. Stratigraphic Column at Glenafric. Approximate location of samples used for age dating are shown by red and blue circles. Red circles represent sand samples for OSL dating and blue circles represent shell samples used for AAR dating (See Figure 11 for location).

AAR ages (ka)									
Species	Site	DL Asp	DL Glu	DL Ile	Asp	Glu	Ile	Average	MIS Sea-level
T.Spissa	Motunau Beach 4	0.509	0.254	0.251	65	58	67	63	3 - 57
T.Spissa	Motunau Beach 7	0.495	0.234	0.281	58	44	85	62	
T.Spissa	Motunau Beach 10	0.500	0.242	0.243	60	49	62	57	
	Average	0.502	0.243	0.259					
T.Spissa	Motanau Beach 2	0.548	0.271	0.287	86	70	89	82	5a - 82
T.Spissa	Motanau Beach 5	0.528	0.265	0.256	75	66	69	70	
T.Spissa	GPS 4.7	0.542	0.265	0.290	83	66	91	80	
	Average	0.539	0.267	0.278					
T.Spissa	MAC-3	0.576	0.279	0.317	104	77	109	97	5c - 96
T.Spissa	Tarapuhi Terrace	0.561	0.300	0.304	94	95	100	96	
T.Spissa	GPS 4.3	0.585	0.271	0.294	110	70	94	92	
	Average	0.574	0.284	0.305					

OSL ages (ka)						
Site	Depth Below Surface (m)	Cosmic Dose Rate (Gy/ka)	Water Content (%)	U(ppm) from 234Th	U(ppm) from 226Ra 214Pb 214Bi	U(ppm) from 210Pb
OSL-MAC	3.5	0.1310 +/- 0.0075	12.5	2.68 +/- 0.24	2.55 +/- 0.15	2.31 +/- 0.20
OSL- GLENAFRICK	6	0.0970 +/- 0.0048	.202	2.22 +/- 0.29	2.09 +/- 0.17	2.03 +/- 0.24
Site	Th(ppm) from 208Tl 212PB 228Ac	K (%)	a-value	De (Gy)	Dose Rate (Gy/ka)	Luminescence Age (ka)
OSL-MAC	8.01 +/- 0.11	1.63 +/- 0.04	0.05 +/- 0.01	314.86 +/- 4.60	3.19 +/- 0.15	98.7 +/- 4.7
OSL- GLENAFRICK	8.71 +/- 0.14	1.99 +/- 0.05	0.05 +/- 0.01	> 728.85 +/- 15.53	3.15 +/- 0.18	> 231.4 +/- 13.9

Table 2. Geochronology Table of AAR and OSL samples. Relevant ages to this study are highlighted in green. Sample locations can be found on the stratigraphic column (Figure 31). Three different amino acids- Asp, Glu, and Ile- were used to estimate the age range for the AAR samples. GPS 4.7 was correlated to a different, but similar, sea level highstand, 5a (~82 ka), than GPS 4.3 and MAC-3 because the amino acid Asp ratio was lower than the other two samples. The OSL sample was obtained from a concurrent study at Penn State and is of similar age (~100 ka) to GPS 4.7 and MAC-3. OSL-Glenafric was not used in this study as its age is much older than the three other relevant samples.

Correlation to the Eustatic Sea Level Curve

Based on the ages from the AAR and OSL samples, terraces could be correlated to eustatic sea levels (Figure 32). Terrace elevations were selected from survey 4 because this survey consisted of all three marine terraces and was the location for all dated samples. When applicable, projected inner edge elevations were assumed to form at mean sea level. However, for terraces without a projected inner edge, GPS survey elevations of erosional surfaces were used for correlation. GPS 4.3 and MAC-3 correlate to MIS sea level 5c and thus the youngest marine terrace, Qt_3 (Figure 28). A line representing Qt_3 was drawn starting at ~71 m above sea level to the sea level highstand MIS 5c. The slope of the line represents the change in elevation over the change in time, resulting in the average uplift rate. Because there was no field evidence indicating a missing marine terrace, each consecutive line was drawn from each terrace elevation from GPS survey 4 to the next MIS sea level highstand. This places Qt_2 at MIS 5e and Qt_1 at MIS 7. The result was parallel lines, indicating a fairly constant uplift rate around GPS survey 4.

Uplift rate was calculated for each terrace using the equation below:

$$\mathbf{Ur = Z_1 - Z_2 - Z_3 / T}$$

Equation 1. Uplift rate calculation (Gardner, 2013).

Ur= uplift rate in m/kyr
Z_1=modern elevation of terrace (m)
Z_2=paleo sea level elevation (m)
Z_3= facies depositional elevation (m)
T= age (ka)

Z_1 is constrained by GPS survey elevations and inner edge projections. Values for this variable are taken from the inner edge estimated elevation, and error in the values is based on the vertical radius of the magenta circles present in the inner edge projections for each GPS survey. Paleo sea elevation values (Z_2) are taken from the eustatic sea level curve highstands that each terrace elevation was correlated to: MIS 5c (Qt_3) at -20m below modern sea level, MIS 5e (Qt_2) at +6m above modern sea level, and MIS 7a (Qt_1) at -12m below modern sea level. Error values are based on the curve range in the eustatic sea level curve (Siddall, 2006). Facies depositional elevations (Z_3) are assigned values based on water depth of marine terrace feature of deposit. Because inner edge projection elevations were used for all but two of the GPS survey points (GPS 1.3 and GPS 1.5), most facies depositional elevation values were assigned a value of 0m as inner edges form at mean sea level. Although several points were not inner edge elevations (GPS 2, GPS 4.13, GPS 4.16, GPS 5, GPS 6.4), these points were assigned facies depositional values of 0m because the points were collected on the terrace tread. GPS 1.3 and 1.5 were assigned values of -1m because each GPS elevation was ~1m below the most adjacent inner edge elevation (GPS 1. 8 at ~33m). The tidal range for Glenafric is ~2m, and thus the range of error for Z_3 is +/-1m. Age values (T) were not taken from shell samples, but the eustatic sea level highstands that each terrace correlated to. However, in the case of Qt_3 (MIS 5c), the age of the sea level highstand at ~100 ka is fairly similar to respective AAR and OSL dates (~96ka and 98.7 ka respectively, see Table 2).

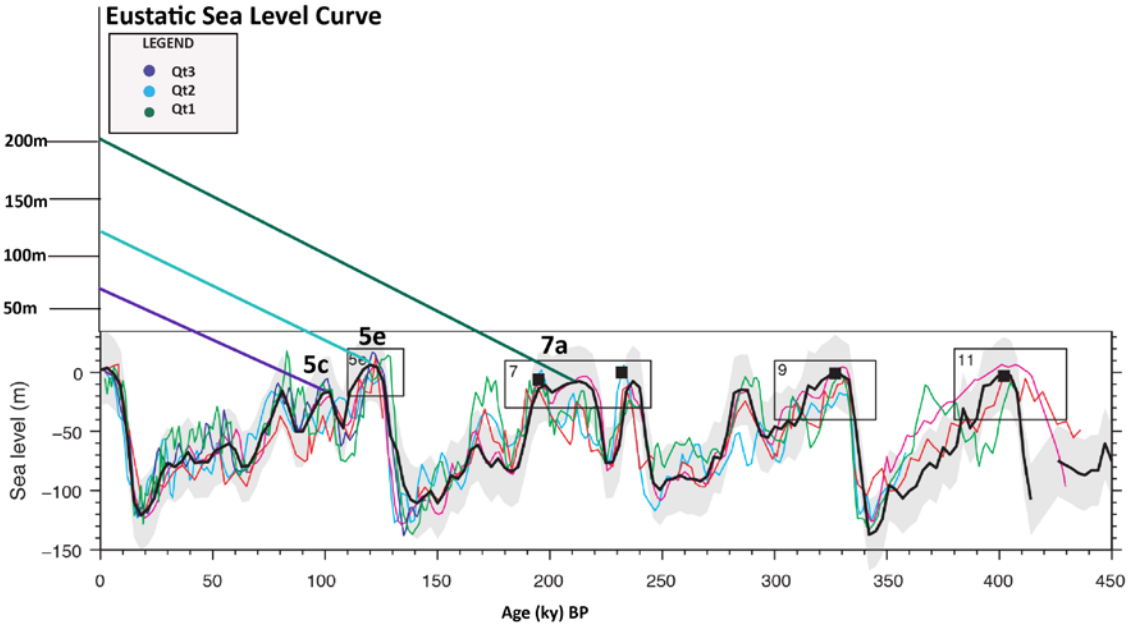

Figure 32. Eustatic sea level curve. Based on the ages from AAR and OSL dating, terrace ages could be correlated to eustatic sea levels. Terrace elevations were selected from GPS survey 4, because survey 4 contained all three marine terraces. Because Qt_3 corresponds to MIS 5c, each consecutive line was drawn to the next sea level high stand. This places Qt_2 at MIS 5e and Qt_1 at MIS 7a, resulting in parallel lines which indicates a fairly constant uplift rate for all three marine terraces at the location of GPS survey 4. Reprinted from (Developments in Quaternary Sciences, 7, Siddall, Eustatic sea level during past interglacials, 2006).

Uplift rates for individual GPS points are given in Table 3. Uplift rate increases with proximity to the structural culmination (located between GPS survey 3- GPS survey 5; see Figure 28). GPS 4.7, 5, 4.13, and 4.16 have some of the highest uplift rates ranging from 0.9-1.0 m/kyr, and lie in the area closest to the structural culmination. The lowest rates of uplift are farthest from the structural culmination and are furthest south: GPS points 1.3, 1.5, 1.8 1.14. and 2 exhibit an uplift rate of .5-.6 m/kyr.

GPS Point	Modern Elevation (m)	Paleo Elevation (m)	Facies Depth (m)	Age (ka)	Uplift Rate (m/kyr)	Distance from Axis (km)
1.5	32 +/- 0.1	-20 +/- 5	-1 +/- 1	100 +/- 5	0.5 +/- 0.1	3.8
1.3	32 +/- 0.2	-20 +/- 5	-1 +/- 1	100 +/- 5	0.5 +/- 0.1	3.8
1.8	33 +/- 7	-20 +/- 5	0 +/- 1	100 +/- 5	0.5 +/- 0.2	4.1
2	40 +/- 4	-20 +/- 5	0 +/- 1	100 +/- 5	0.6 +/- 0.1	5.7
3.6	53 +/- 8	-20 +/- 5	0 +/- 1	100 +/- 5	0.7 +/- 0.2	6.2
4.7	71 +/- 4	-20 +/- 5	0 +/- 1	100 +/- 5	0.9 +/- 0.2	4.9
5	84 +/- 5	-20 +/- 5	0 +/- 1	100 +/- 5	1.0 +/- 0.2	3.5
6.2	110 +/- 10	-20 +/- 5	0 +/- 1	100 +/- 5	1.3 +/- 0.2	2.7
GPS Point	Modern Elevation (m)	Paleo Elevation (m)	Facies Depth (m)	Age (ka)	Uplift Rate (m/kyr)	Distance from Axis (km)
1.14	79 +/- 3	6 +/- 3	0 +/- 1	120 +/- 5	0.6 +/- 0.1	3.9
4.13	123 +/- 3	6 +/- 3	0 +/- 1	120 +/- 5	1.0 +/- 0.1	4.2
GPS Point	Modern Elevation (m)	Paleo Elevation (m)	Facies Depth (m)	Age (ka)	Uplift Rate (m/kyr)	Distance from Axis (km)
4.16	194 +/- 2.5	-10 +/- 5	0 +/- 1	210 +/- 10	1.0 +/- 0.1	3.9
6.4	198 +/- 3.3	-10 +/- 5	0 +/- 1	210 +/- 10	1.0 +/- 0.1	2.2

Table 3. Calculated uplift rates for individual GPS points. Points highlighted in pink are the values used for eustatic sea level highstand correlation (Figure 32).

Discussion

The goal of this study is to relate the local variations in rate of uplift of marine terraces to fold growth along the NCFTB in order to understand how fold growth contributes to local uplift. The methods used to obtain this goal are outlined below:

- Determine marine terrace inner edge elevations using DGPS surveys, LIDAR, and 10m DEM data.
- Define marine terrace boundaries.
- Assign ages to marine terraces using samples collected for AAR and OSL dating.
- Calculate the local uplift rate of marine terraces.

So far this study has provided evidence of the following:

- Inner edge elevations using cross-sections constructed from DGPS surveys and topographic profiles created using LIDAR and the 10m DEM (Figures 12, 15, 16, 18, 21, and 23). These inner edges have helped to define terrace boundaries and the elevations used for calculating uplift rate.
- Extent of marine terraces (Figure 28).
- Evidence of coastal southward tilting from topographic profiles along the coast (Figures 6 and 25). Figure 2 shows that folds and faults in the NCFTB, including the Cass anticline and Hamilton Fault plunge to the southwest, underneath the Quaternary alluvium and marine sediment cover.

- Correlation to Cass and Montserrat anticlinal axes using inner edge elevations and distances to the anticline (Figures 29 and 30). Generally, the points closest to the anticlinal axis were at a higher elevation, although several points from GPS Survey 1 (the southernmost survey) did not support this observation. Because the majority of outliers were present in the southernmost field area and the correlation between uplift rate and distance from the Cass anticline was weak, this indicated that other factors had an influence on marine terrace uplift rate, such as proximity to the structural culmination. Offshore fold stratigraphic sequences support the idea that folding and coastal uplift have occurred continuously but variably throughout the past 0.75 years (Barnes 1995, 2011) as well.
- AAR and OSL techniques dated Qt_3 at ~ 100 ka, at MIS sea level 5c. This age provided a starting point for eustatic sea level correlation and uplift rate calculation.
- Uplift rates generally decrease to the southwest (Table 3). However, uplift rates were highest between GPS surveys 4-6 which were closest in distance to the structural culmination (See Figure 28 for locations).

Fold Influence on Marine Terraces

In simple terms, as the Hamilton thrust fault as well as some doubly plunging local thrust faults propagate toward the southwest, the Cass anticline and other local folds grow and propagate to the southwest as well (See Figure 5). Figure 33 shows the evolution of the influence of the Hamilton fault on the Cass anticline fold growth. As the Hamilton fault continues to develop, accumulate slip, and propagate southward (due to oblique motion from tectonic plate migration), it begins to thrust rock layers on top of one another creating the beginning of the Cass anticline. The anticline continues to grow in elevation and propagate in the direction of fault propagation, southwest. Eventually, anticlinal growth uplifts the marine terraces and effects marine terrace orientation (tilt). The topographic profiles support fault and fold influence on marine terrace uplift as topographic profiles G-H (Figure 25) exhibit moderate southward tilting decreasing in elevation from ~100m to 60m, consistent with the direction of fault propagation (See Figure 2).

Figure 29 and Table 3 show that proximity to an anticlinal axis, in this case the Cass anticline, has an influence on marine terrace uplift. GPS 4.16, 5.1 and 6.2 are all less than 4km away from the anticlinal axis and exhibit the highest uplift rates of 1.0 and 1.3 m/kyr respectively (See Table 3; Figure 34). However, proximity to the anticlinal axis is not the greatest factor in marine terrace uplift. GPS 1.3, 1.5, and 1.8, the southernmost points in the field area, are also less than 4 km away from the anticlinal axis, yet exhibit the lowest uplift rates of 0.5 m/kyr (Table 3; Figure 34).

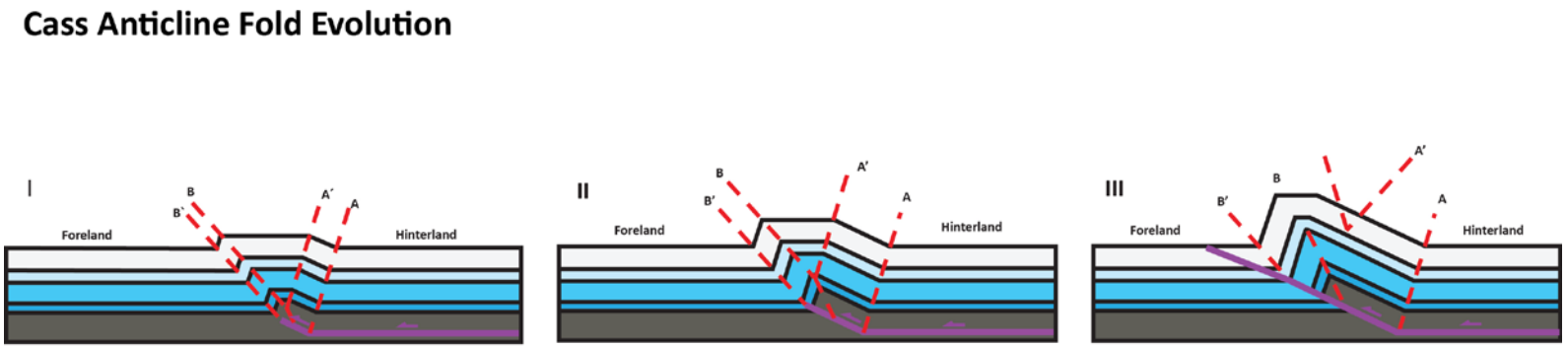

Figure 33. Sequential model of fault-propagation-fold evolution as the Cass Anticline propagates southwestward. The view is perpendicular to the coast. Republished with permission of *Eclogae Geologicae Helvetiae,* from (Geometry and kinematics of fault-propagation folding, Suppe and Medwedeff, 83, 3, 1990), permission conveyed through Copyright Clearance Center, Inc. Modified from Hill and Surpless (2014).

Why is it that GPS 1.3 and 1.5 are the same distance away from the anticlinal axis as GPS 4.16 and 6.2, yet experience the lowest uplift rate? Figures 5 and 28 show the location of the structural culmination of the Cass anticline (Ktp) and the structural culmination of the Montserrat anticline (Ike). The structural culmination exposes the oldest formation, in the case of the Cass anticline, the basement rock of the Pahua Torlesse, at the highest point of the anticlinal axis. Because the Pahua Torlesse is present at the structural culmination, this means that uplift has exposed the deepest bedrock and therefore, the structural culmination represents the location with the most accumulated fault slip and the greatest amount of uplift for the longest period of time. Table 3 shows that the GPS points included in surveys 3-4 have some of the highest uplift rates ranging from 0.7-1.0 m/kyr. Furthermore, the points used in the eustatic sea curve correlation, all from survey 4, have the same uplift rate ~1.0 m/kyr, due to their proximity to the structural culmination. GPS 6.2 and 6.4 also exhibit some of the highest uplift rates ranging from 1.0-1.3 m/kyr (Table 3) and are a little over 2 km from the structural culmination of the Montserrat anticline.

However, proximity to the anticlinal axis or structural culmination are not the only factors that affect marine terrace uplift. The older the terrace, the longer it has been exposed to anticlinal growth and therefore experiences more uplift. The amount of uplift a terrace experiences is shown by terrace elevation. GPS 4.16 and GPS 6.4 from Qt_1, the oldest terrace, were surveyed at ~194 and ~198m in elevation respectively, as compared to the elevations of GPS 1.14 (84m) and GPS 4.13 (135m) from the next oldest terrace, Qt_2. Therefore,

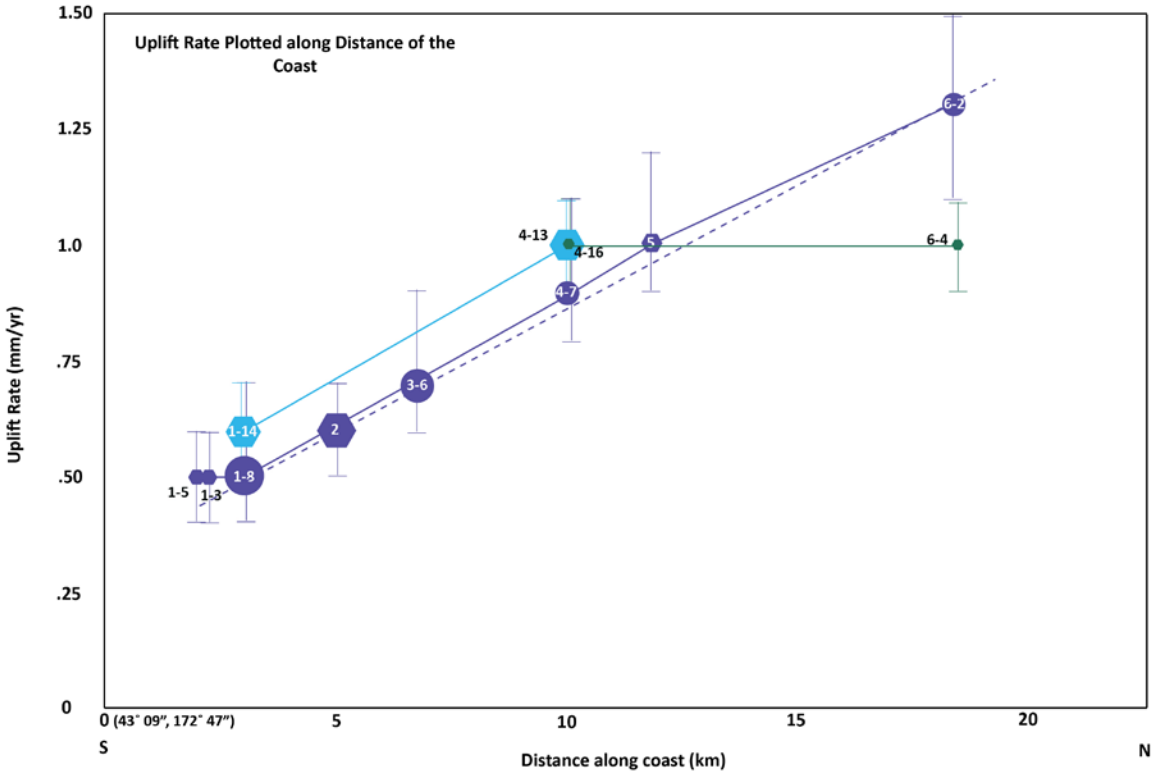

Figure 34. Uplift rate changes with distance along the coast. Higher uplift rates are generally located in the northern region of the field area. The highest uplift rates (1.0-1.3 m/kyr) belong to points from GPS surveys 3-4, the surveys in closest proximity to the structural culmination (See Figures 5 and 28); or to surveys 5-6, in the northernmost region of the field area.

Conclusions

Several factors affect the local uplift of marine terraces: proximity to the anticlinal axis, proximity to the structural culmination, and amount of time exposed to fold growth. In summary, fault and fold propagation is the primary influence on terrace uplift (Figure 35). Anticlinal growth is the mechanism for local uplift, tilting in the direction of fault propagation. As the Hamilton Fault propagates to the southwest, the Cass anticline grows to the southwest, tilting the terraces in the direction of propagation. Hence, elevations in the north have been under the influence of anticlinal uplift the longest and therefore have higher inner edge and erosional surface elevations. Proximity to the anticlinal axis and structural culmination serve as stronger influence on marine terrace uplift as the greatest amount of uplift occurs at the structural culmination and is reflected in the terraces closest in distance to the structural axis.

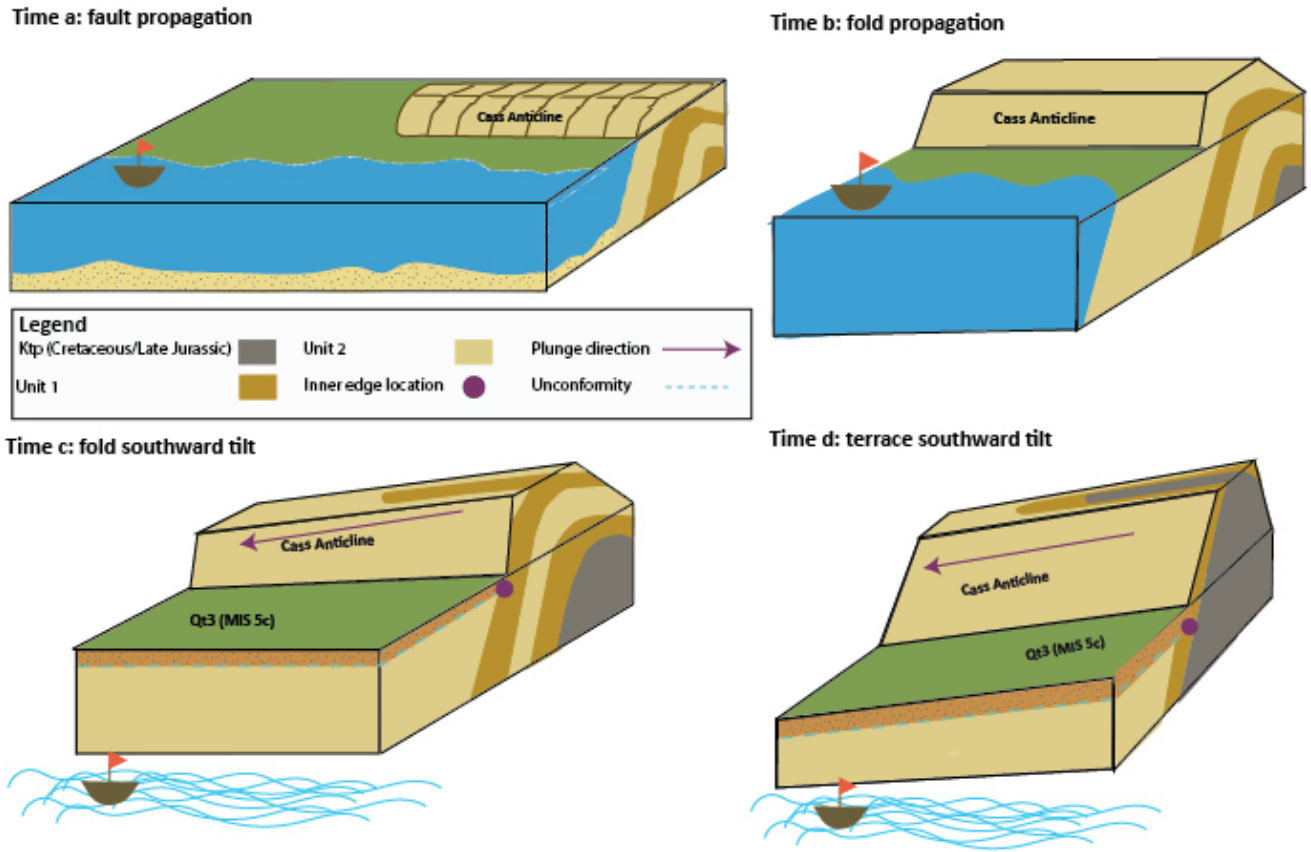

Figure 35. The sequence of fault and fold propagation. The Hamilton fault is not included in the diagram as it represents a blind thrust fault, a fault that characterized the NCFTB. Time a: The Hamilton Fault has begun to propagate towards the southwest following plate migration. The Cass Anticline is just beginning to grow. Time b: the Cass anticline begins to propagate and grow above the surface. Figure only shows the axis of the fold, so the Hamilton Fault is too far beneath the sediment to see. Time c: beginning of fold tilt toward the southwest following the direction of fault propagation. Time d: Cass anticline's influence on terrace tilt and uplift as the marine terrace beings to tilt toward the southwest in the direction of fault and fold propagation.

Summary

The use of AAR and OSL dating of shell and sand samples, DGPS surveys, inner edge projections, and uplift rates calculated from the eustatic sea level curve all helped to quantify the effects of local fault and fold growth in the Glenafric region. Correlation of inner edge elevations to the sea level highstands of the eustatic sea level curve helped to date terraces in chronological order of ~210, ~120, and ~100 ka; and helped to calculate uplift rate along the coast with the highest uplift rate of 1.3 m/kyr in the northernmost region of the field area and 0.5 m/kyr in the southernmost region of the field. Calculated uplift rates and topographic profiles that were plotted along the coast provided evidence of marine terrace tilting towards the southwest, following the direction of local fault thrust (Hamilton Fault) and local fold (Cass anticline) propagation. The distance between inner edge elevations and anticlinal axes showed that inner edges closest to the axes generally had a higher uplift rate. However, upon further observation of the location of the highest uplift rates (1.0-1.3 m/kyr), it was determined that proximity to the structural culmination of the Cass and Montserrat anticlines as well as terrace age have a more significant impact on marine terrace uplift than proximity to the anticlinal axis.

References

Barnes, P. (1995). “High-frequency sequences deposited during Quaternary sea-level cycles on a deforming continental shelf, North Canterbury, New Zealand,” Sedimentary Geology.

Barnes, P. (1996). “Active folding of Pleistocene unconformities on the edge of the Australia-Pacific plate boundary zone, offshore North Canterbury, New Zealand,” Tectonics.

Barnes, P. (2011). “Submarine faulting beneath Pegasus Bay, offshore Christchurch,” NIWA report on short-term Canterbury Earthquake Recovery Project.

Carr, M. (1970). “The Stratigraphy and Chronology of the Hawera Series Marginal Marine Succession of the North Canterbury Coast,” Thesis, University of Canterbury.

Covault, A. (2004). “Deformation along the margin of the North American plate in north central California between Alder Creek and Mendocino as recorded by Quaternary marine terraces,” Trinity University.

Demets, C. (2010). “Geologically current plate motions,” *Geophysics Journal International,* 181.

Furlong, K., and Kemp, P. (2009). “The lithospheric geodynamics of plate boundary transpression in New Zealand: Initiating and emplacing subduction along the Hikurangi margin, and the tectonic evolution of the Alpine Fault system,” *Tectonophysics.*

Gardner, T. (1992). “Quaternary uplift astride the aseismic Cocos Ridge, Pacific Coast, Costa Rica.”

Gardner, T. (2012). Personal Communication.

Gardner, T. (2013). “Upper-plate deformation in response to flat slab subduction inboard of the aseismic Cocos Ridge, Osa Peninsula, Costa Rica,” *Lithosphere,* 5, 3.

Hill, N., and Surpless, B. (2014). “Analysis of finite fold geometry and variations in strain based on structural position: a case study from the Stillwell Anticline, west Texas,” Abstracts with Programs, Southcentral GSA, Vancouver, British Columbia.

Matsu’ura, T. (2013). “Late Quaternary uplift rate inferred from marine terraces, Shimokita Peninsula, northeastern Japan: A preliminary investigation of the buried shoreline angle,” *Geomorphology*.

Matsu’ura T. (2015). “Late Quaternary uplift rate inferred from marine terraces, Muroto Peninsula, southwest Japan: Forearc deformation in an oblique subduction zone,” *Geomorphology.*

Ota, Y. (1996). “Pleistocene terraces of Kaikora Peninsula and the Marlborough Coast*,” New Zealand Journal of Geology and Geophysics.*

Siddall, M. (2006). “Eustatic sea level during past interglacials,” *Developments in Quaternary Sciences,* 7.

Suppe, J., and Medwedeff, D. (1990). “Geometry and kinematics of fault-propagation folding,” *Eclogae Geologicae Helvetiae* 83, 3.

Walcott, R. (1998). “Modes of oblique compression: late Cenozoic tectonics of the South Island of New Zealand,” *Reviews of Geophysics,* 36, 1.

Yousif, H. (1987). “The application of remote sensing to geomorphological neotectonic mapping in North Canterbury, New Zealand,” thesis, University of Canterbury.

GIS Data References

Geo Information Solutions Report (2003).

GNS Science (2014). http://www.gns.cri.nz/Home/Our-Science/Earth-Science/Regional-Geology/Geological-Maps/1-250-000-Geological-Map-of-New-Zealand-QMAP/Digital-Data-and-Downloads

LINZ Data Service (2014). https://data.linz.govt.nz/

Appendix: Raw GPS Data

GPS Survey 1

Point_ID	Elevation (m)	Vertical Error	Horizontal Error	Easting	Northing	Comment
1	58.958	0.1	0.1	1583707.25	5223841.92	tread possibly
2	50.739	0.1	0.1	1583664.71	5223863.07	some sort of unconformity
3	31.803	0.2	0.2	1584601.99	5224494.67	unconformity
4	40.996	0.7	0.4	1584636.80	5224494.56	marine sed thickness top tread
5	32.068	0.1	0.1	1584604.04	5224488.11	retake
6	2.67	0.8	0.6	1584997.25	5224490.37	holocene inner edge
7	22.737	0.6	1.2	1584983.94	5224516.71	riser
8	32.643	0.5	0.6	1584973.63	5224526.21	unconformity
9	45.44	0.9	0.4	1584954.78	5224586.38	tread thickness
10	49.968	0.6	0.5	1584965.03	5224632.81	inner edge
11	71.124	12	6.3	5224727.695	1584923.669	yousif m2?
12	84.815	11.3	6.3	5224771.05	1584960.936	unconformity
13	92.51	10	5.9	5224795.024	1584982.476	top tread thickness
14	84.184	10.6	5.9	5224917.922	1584986.784	unconformity
15	89.39	13.9	6.5	5225030.196	1585012.164	unconformity
16	104.806	13.2	6	5225101.594	1585022.047	tread thickness of m4?
17	123.175	9.8	6	5225215.693	1585033.015	M4? inner edge
18	145.346	9.6	5.9	5225368.407	1585039.543	highest tread
19	42.029	8.9	6	5224630.952	1584704.374	unconformity m1?
20	48.868	10.6	8.3	5224917.116	1584116.201	river terrace unconformity
21	102.884	8.8	6	5225218.47	1583157.113	unconformity marine

GPS Survey 3

Point ID	**Elevation (m)**	**Vertical Error**	**Horizontal Error**	**Easting**	**Northing**	**Comment**
1	**40.271**	**0.4**	**0.2**	**1588538.8**	**5226076.86**	**bedrock unconformity**
2	**62.909**	**0.5**	**0.2**	**1588503.7**	**5226043.47**	**thickness of marine cover mis5**
3	**44.019**	**0.5**	**0.3**	**1588477.96**	**5225940.41**	
4	**41.449**	**0.6**	**0.2**	**1588443.91**	**5225886.88**	
5	**57.148**	**0.3**	**0.1**	**1588457.59**	**5225908.11**	**ht of marine sed tread**
6	**53.782**	**1.2**	**0.6**	**1588416.07**	**5226236.01**	**unconformity**
7	**89.291**	**0.2**	**0.1**	**1588576.54**	**5226589.03**	
8	**68.862**	**0.7**	**0.9**	**1588972.99**	**5227283.59**	

GPS Survey 4

Point ID	Elevation (m)	Vertical Error	Horizontal Error	Easting	Northing	Comment
1	56.579	3.2	1.8	1590294.86	5227877.82	unconformity
2	71.587	3.5	2	1590260.12	5227899.97	m1 tread at seacliff
3	58.696	4.7	2.7	1590189.09	5227939.34	AAR sample
4	73.956	3.9	1.5	1590203.29	5227982.59	m1 tread 2
5	74.741	2.9	1.3	1590134.97	5228084.7	m1 tread
6	53.917	8.8	3	1590073.5	5228121.1	
7	61.46	4.5	2.7	1589936.9	5228169.95	AAR sample
8	76.99	3.1	2.2	1589965.63	5228277.06	m1 tread
9	84.727	4.1	2.9	1590160.86	5228549.1	colluvial riser to m2
10	92.17	5	3.1	1590195.27	5228789.85	
11	102.752	4.8	3.7	1590179.52	5228850.5	
12	119.42	6.9	4.5	1590151.54	5228907.39	
13	135.626	5	2.8	1590071.08	5228988.06	
14	151.133	1.8	1.1	1590024.27	5229063.43	
15	171.518	2.5	1.6	1589996.03	5229124.53	
16	193.919	2.5	1.6	1589934.19	5229170.89	

GPS Survey 5

Point ID	Elevation (m)	Vertical Error	Horizontal Error	Easting	Northing	Comment
1	83.97	5	1.5	1592092.64	5228695.85	unconformity question

GPS Survey 6

Point ID	Elevation (m)	Vertical Error	Horizontal Error	Easting	Northing	Comment
1	127.312	4.9	2.6	1597935.75	5230836.03	marine sed
2	100.305	4.4	2.3	1598183.61	5230866.02	hor marine bed knickpt
3	185.632	3.3	1.3	1598004.89	5231302.64	terrace tread eroded
4	198.604	3.3	1.3	1598060.05	5231450.32	near inner edge